New Mode of Coordination for the Dinitrogen Ligand: Formation, Bonding, and Reactivity of a Tantalum Complex with a Bridging N_2 Unit That Is Both Side-On and End-On

Michael D. Fryzuk,*,† Samuel A. Johnson,† Brian O. Patrick,†,⊥ Alberto Albinati,‡ Sax A. Mason,§ and Thomas F. Koetzle||

Contribution from the Department of Chemistry, University of British Columbia, 2036 Main Mall, Vancouver, B.C., Canada V6T 1Z1, Istituto di Chimica Farmaceutica, Università di Milano, 42 Viale Abruzzi, I-20131 Milano, Italy, Institut Max von Laue-Paul Langevin, 38042 Grenoble Cedex 9, France, and Department of Chemistry, Brookhaven National Laboratory, P.O. Box 5000, Upton, New York, 11973-5000

Received December 1, 2000

Abstract: The reaction of a mixture of 1 equiv of $PhPH_2$ and 2 equiv of $PhNHSiMe_2CH_2Cl$ with 4 equiv of Bu^nLi followed by the addition of THF generates the lithiated ligand precursor $[NPN]Li_2\cdot(THF)_2$ (where [NPN] = $PhP(CH_2SiMe_2NPh)_2$). The reaction of $[NPN]Li_2\cdot(THF)_2$ with $TaMe_3Cl_2$ produces $[NPN]TaMe_3$, which reacts under H_2 to yield the diamagnetic dinuclear Ta(IV) tetrahydride $([NPN]Ta)_2(\mu\text{-}H)_4$. This hydride reacts with N_2 with the loss of H_2 to produce $([NPN]Ta(\mu\text{-}H))_2(\mu\text{-}\eta^1\text{:}\eta^2\text{-}N_2)$, which was characterized both in solution and in the solid state, and contains strongly activated N_2 bound in the unprecedented side-on end-on dinuclear bonding mode. A density functional theory calculation on the model complex $[(H_3P)(H_2N)_2Ta(\mu\text{-}H)]_2(\mu\text{-}\eta^1\text{:}\eta^2\text{-}N_2)$ provides insight into the molecular orbital interactions involved in the side-on end-on bonding mode of dinitrogen. The reaction of $([NPN]Ta(\mu\text{-}H))_2(\mu\text{-}\eta^1\text{:}\eta^2\text{-}N_2)$ with propene generates the end-on bound dinitrogen complex $([NPN]Ta(CH_2CH_2CH_3))_2(\mu\text{-}\eta^1\text{:}\eta^1\text{-}N_2)$, and the reaction of $[NPN]Li_2\cdot(THF)_2$ with $NbCl_3(DME)$ generates the end-on bound dinitrogen complex $([NPN]NbCl)_2(\mu\text{-}\eta^1\text{:}\eta^1\text{-}N_2)$. These two end-on bound dinitrogen complexes provide evidence that the bridging hydride ligands are responsible for the unusual bonding mode of dinitrogen in $([NPN]Ta(\mu\text{-}H))_2(\mu\text{-}\eta^1\text{:}\eta^2\text{-}N_2)$. The dinitrogen moiety in the side-on end-on mode is amenable to functionalization; the reaction of $([NPN]Ta(\mu\text{-}H))_2(\mu\text{-}\eta^1\text{:}\eta^2\text{-}N_2)$ with $PhCH_2Br$ results in C−N bond formation to yield $[NPN]Ta(\mu\text{-}\eta^1\text{:}\eta^2\text{-}N_2CH_2Ph)(\mu\text{-}H)_2TaBr[NPN]$. Nitrogen-15 NMR spectral data are provided for all the tantalum−dinitrogen complexes and derivatives described.

Introduction

Serendipity has figured prominently in the synthesis of dinitrogen complexes, from the first reported dinitrogen complex, $[Ru(NH_3)_5N_2]^{2+}$,[1,2] to the recent reports of the cleavage of dinitrogen.[3−7] Out of the hundreds of dinitrogen derivatives that have been prepared either rationally or via serendipity, only a handful have displayed reactivities that result in functionalization of the coordinated dinitrogen,[8−16] and the majority of these are early transition metal complexes that require strongly reducing conditions for their synthesis. Although a few catalytic processes have been reported none are commercially interesting largely because of the presence of stoichiometric quantities of reducing agent.[17] Clearly, any commercially viable process that functionalizes dinitrogen under mild conditions will require activation via coordination to a metal complex and this step must be facile.

We recently reported the discovery of a facile process for the preparation of early transition metal dinitrogen complexes. The reaction of dihydrogen with the tantalum(V) derivative $[NPN]TaMe_3$ (where [NPN] = $PhP(CH_2SiMe_2NPh)_2$) generates the dinuclear tetrahydride $([NPN]Ta)_2(\mu\text{-}H)_4$ that reacts spontaneously with N_2 to generate $([NPN]Ta)_2(\mu\text{-}H)_2(\mu\text{-}\eta^1\text{:}\eta^2\text{-}N_2)$, a complex with the dinitrogen unit end-on bound to one tantalum

† University of British Columbia.
⊥ Professional Officer: UBC X-ray Structural Laboratory.
‡ Università di Milano.
§ Institut Max von Laue-Paul Langevin.
|| Brookhaven National Laboratory.

(1) Allen, A. D.; Senoff, C. V. *Chem. Commun.* **1965**, 621.
(2) Senoff, C. V. *J. Chem. Educ.* **1990**, *67*, 368.
(3) LaPlaza, C. E.; Cummins, C. C. *Science* **1995**, *268*, 861.
(4) LaPlaza, C. E.; Johnson, M. J. A.; Peters, J. C.; Odom, A. L.; Kim, E.; Cummins, C. C.; George, G. N.; Pickering, I. J. *J. Am. Chem. Soc.* **1996**, *118*, 8623.
(5) Laplaza, C. E.; Johnson, A. R.; Cummins, C. C. *J. Am. Chem. Soc.* **1996**, *118*, 709.
(6) Clentsmith, G. K. B.; Cloke, F. G. H. *J. Am. Chem. Soc.* **1999**, *121*, 10444.
(7) Caselli, A.; Solari, E.; Scopelliti, R.; Floriani, C.; Re, N.; Rizzoli, C.; Chiesi-Villa, A. *J. Am. Chem. Soc.* **2000**, *122*, 3652−3670.
(8) Richards, R. L. *Pure Appl. Chem.* **1996**, *68*, 1521.
(9) Tuczek, F.; Lehnert, N. *Angew. Chem., Int. Ed. Engl.* **1998**, *37*, 2636.
(10) Leigh, G. J. *Science* **1998**, *279*, 506.
(11) Hidai, M.; Mizobe, Y. *Chem. Rev.* **1995**, *95*, 1115.
(12) Hidai, M.; Mizobe, Y. *Reactions of coordinated dinitrogen and related species*; Braterman, P. S., Ed.; Plenum Press: New York, 1989; Vol. 2, p 53.
(13) Henderson, R. A. *Transition Met. Chem.* **1990**, *15*, 330.
(14) Fryzuk, M. D.; Johnson, S. A. *Coord. Chem. Rev.* **2000**, *200−202*, 379−409.
(15) Dilworth, J. R.; Richards, R. L. *Reactions of Dinitrogen Promoted by Transition Metal Complexes*; Wilkinson, G., Stone, F. G. A., Abel, E. W., Ed.; Pergamon Press: Oxford, 1982; Vol. 8, p 1073.
(16) Gambarotta, S. *J. Organomet. Chem.* **1995**, *500*, 117.
(17) Oshita, H.; Mizobe, Y.; Hidai, M. *J. Organomet. Chem.* **1993**, *456*, 213−220.

10.1021/ja0041371 CCC: $20.00
Published on Web 04/05/2001

Scheme 1

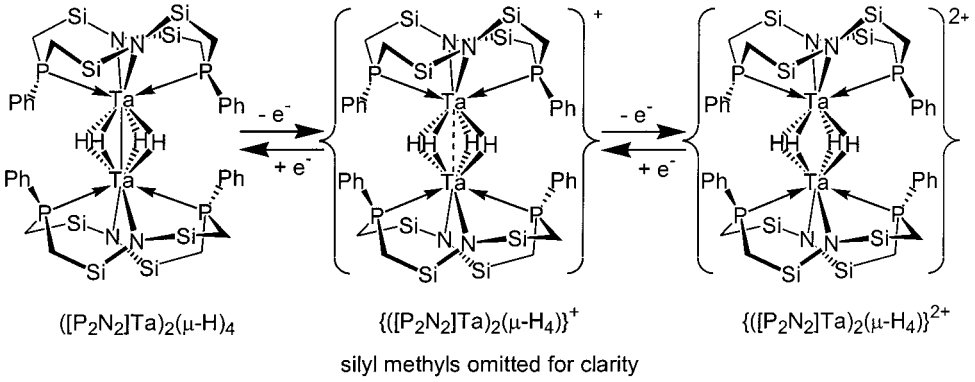

center and side-on bound to the other tantalum center.[18] This process is remarkable for several reasons: (i) the reduction of the dinitrogen moiety occurs via reductive elimination of H_2, so that no strong reducing agent is required in the formation of this dinitrogen complex from a tantalum(V) precursor, and (ii) unlike many other dinitrogen complexes formed by the reductive elimination of H_2 from one or more transition metal centers,[19−23] the dinitrogen moiety in this complex is activated toward further functionalization. In this paper we discuss the full details of the synthesis of $([NPN]Ta)_2(\mu\text{-}H)_2(\mu\text{-}\eta^1{:}\eta^2\text{-}N_2)$, some of the reactivity patterns of the $Ta_2(\mu\text{-}H)_2(\mu\text{-}\eta^1{:}\eta^2\text{-}N_2)$ unit, and a description of the bonding in this unique example of an end-on side-on bound dinitrogen complex.

Results and Discussion

Our recent published work on tantalum chemistry has focused on transformations of $[P_2N_2]TaMe_3$,[24,25] where $[P_2N_2] = PhP(CH_2SiMe_2NSiMe_2CH_2)_2PPh$,[26] a macrocyclic ligand with two amido and two phosphine donors. Many of the tantalum complexes prepared with this $[P_2N_2]$ ligand are unreactive. For example, the dinuclear Ta(IV) tetrahydride $([P_2N_2]Ta)_2(\mu\text{-}H)_4$ is coordinatively saturated and does not bind and activate small molecules; however, the electrons stored in the tantalum−tantalum bond of this complex allow it to behave as a reducing agent, as shown in Scheme 1.[25]

To produce more reactive systems we investigated a new ligand system in which one of the phosphine donors was removed to generate a tridentate donor set. It was anticipated that enhanced reactivity would result with [NPN] systems as compared to $[P_2N_2]$ analogues simply because the former must be more coordinatively unsaturated.

Synthesis and Characterization of $[PhP(CH_2SiMe_2NPh)_2]Li_2\cdot(THF)_2$ (1). A convenient route to the lithiated [NPN] ligand precursor is shown in Scheme 2.[27] The silylated aniline $ClCH_2SiMe_2NHPh$ is prepared by the reaction of LiNHPh with $ClCH_2SiMe_2Cl$. The reaction of 4 equiv of Bu^nLi with a mixture of 2 equiv of $ClCH_2SiMe_2NHPh$ and 1 equiv of $PhPH_2$ in diethyl ether was expected to provide $[NPN]Li_2$, after separation of the LiCl by filtration; however, this species proved difficult to characterize. An easily isolated lithiated ligand precursor is prepared via the addition of approximately 4 equiv of THF to a slurry of the presumed $[NPN]Li_2$ crude product in hexanes. The solid immediately dissolves, and later precipitates in 85% yield as a colorless crystalline solid identified by ^1H, $^{31}P\{^1H\}$, and $^7Li\{^1H\}$ NMR spectroscopies, elemental analysis, and X-ray crystallography (see Supporting Information) as $[NPN]Li_2\cdot(THF)_2$ (**1**).

Scheme 2

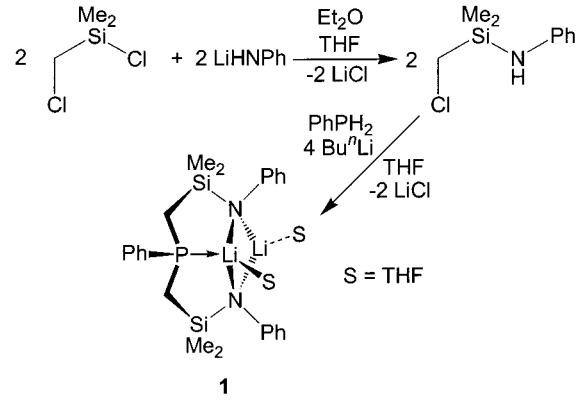

1

Synthesis and Characterization of $[NPN]TaMe_3$ (2). The synthesis of $[NPN]TaMe_3$ was accomplished by the reaction of **1** with $TaMe_3Cl_2$, as shown in eq 1. Complex **2** is a pale yellow light-sensitive solid that was isolated in 80% yield.

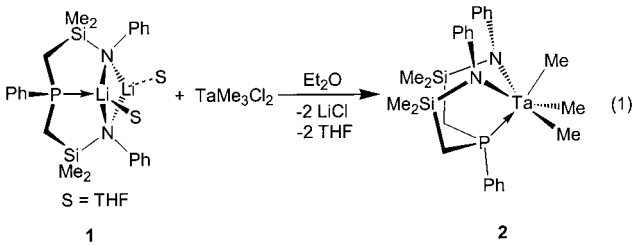

An ORTEP depiction of the solid-state molecular structure of **2** as determined by X-ray crystallography is shown in Figure 1 and crystal data are given in Table 1. The [NPN] ligand in **2**

(18) Fryzuk, M. D.; Johnson, S. A.; Rettig, S. J. *J. Am. Chem. Soc.* **1998**, *120*, 11024−11025.
(19) Sacco, A.; Rossi, M. *J. Chem. Soc., Chem. Commun.* **1967**, 316.
(20) (a) de Wolf, J. M.; Blaauw, R.; Meetsma, A.; Teuben, J. H.; Gyepes, R.; Varga, V.; Mach, K.; Veldma, N.; Spek, A. L. *Organometallics* **1996**, *15*, 5, 4977. (b) Chirik, P. J.; Henling, L. M.; Bercaw, J. E. *Organometallics* **2001**, *20*, 534−544.
(21) Vigalok, A.; Ben-David, Y.; Milstein, D. *Organometallics* **1996**, *15*, 1839.
(22) Osman, R.; Pattison, D. L.; Perutz, R. N.; Bianchini, C.; Casares, J. A.; Peruzzini, M. *J. Am. Chem. Soc.* **1997**, *119*, 8459.
(23) Morris, R. H. *Inorg. Chem.* **1992**, *31*, 1471.
(24) Fryzuk, M. D.; Johnson, S. A.; Rettig, S. J. *Organometallics* **1999**, *18*, 4059−4067.
(25) Fryzuk, M. D.; Johnson, S. A.; Rettig, S. J. *Organometallics* **2000**, *19*, 3931−3941.
(26) Fryzuk, M. D.; Love, J. B.; Rettig, S. J. *J. Chem. Soc., Chem. Commun.* **1996**, 2783.
(27) Schrock, R. R.; Seidel, S. W.; Schrodi, Y.; Davis, W. M. *Organometallics* **1999**, *18*, 428−437.

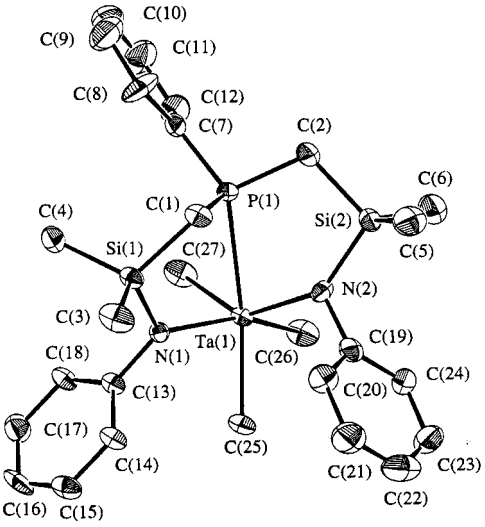

Figure 1. ORTEP depiction of the solid-state molecular structure of [NPN]$TaMe_3$ (**2**) as determined by X-ray crystallography. Selected bond lengths (Å) and bond angles (deg): Ta(1)−P(1), 2.7713(13); Ta(1)−N(1), 2.078(4); Ta(1)−N(2), 2.025(4); Ta(1)−C(25), 2.224(5); Ta(1)−C(26), 2.228(5); Ta(1)−C(27), 2.204(5); N(1)−Ta(1)−N(2), 113.0(2); P(1)−Ta(1)−N(1), 81.72(11); P(1)−Ta(1)−N(2), 70.3(1); P(1)−Ta(1)−C(25), 160.74(14); P(1)−Ta(1)−C(26), 119.28(15); P(1)−Ta(1)−C(27), 78.94(15); N(1)−Ta(1)−C(25), 82.6(2); N(1)−Ta(1)−C(26), 152.4(2); N(1)−Ta(1)−C(27), 89.6(2); N(2)−Ta(1)−C(25), 106.0(2); N(2)−Ta(1)−C(26), 92.0(2); N(2)−Ta(1)−C(27), 137.7(2); C(25)−Ta(1)−C(26), 79.3(2); C(25)−Ta(1)−C(27), 112.2(2); C(26)−Ta(1)−C(27), 78.2(2).

Table 1. X-ray Diffraction Crystal Data and Structure Refinement for [NPN]$Li_2(C_4H_8O)_2$ (1), [NPN]$TaMe_3$ (2), and ([NPN]Ta(μ-H))$_2$(μ-η^1:η^2-N_2) (**4**)

compound	**2**[a]	**4**[a]
formula	$C_{33}H_{46}N_2P_2Si_2Ta$	$C_{48}H_{64}N_6P_2Si_4Ta_2$
fw	738.83	1261.26
color, habit	yellow, block	brown, block
cryst size, mm	0.15 × 0.35 × 0.50	0.50 × 0.20 × 0.20
cryst syst	orthorhombic	monoclinic
space group	*Pna*2$_1$ (No. 33)	*P*2$_{1/n}$ (No. 14)
a, Å	22.1812(3)	13.2532(4)
b, Å	8.6093(3)	19.3894(3)
c, Å	18.0832	21.4134(2)
α, deg		
β, deg		95.9773(6)
γ, deg		
V, Å^3	3453.25(11)	5472.7(2)
Z	4	4
T, °C	−93	20
ρ_{calc}, g/cm^3	1.42	1.53
F(000)	1496.00	2504.00
radiation	Mo	Mo
μ, cm^{-1}	33.17	41.73
transmission factors	0.4463−1.000	0.6218−1.0000
$2\theta_{max}$, deg	60.0	55.8
total no. of reflns	29324	48443
no. of unique reflcns	5245	12845
R_{merge}	0.039	0.065
no. with $I \geq n\theta(I)$	5994 ($n = 3$)	12473 ($n = 0$)
no. of variables	351	559
R	0.031[a]	0.065[a]
R_w	0.024[a]	0.090[a]
GOF	1.71	1.01
max Δ/σ	0.04	0.01
residual density, e/Å^3	0.69, −0.72	2.71, −2.68

[a] Rigaku/ADSC CCD diffractometer, $R = \sum||F_o^2| - |F_c^2||/\sum|F_o^2|$; $R_w = (\sum w(|F_o^2| - |F_c^2|)^2/\sum w|F_o^2|^2)^{1/2}$.

is facially bound and the methyl groups are all cis disposed. The overall geometry at the tantalum center is very distorted. The P(1) atom is approximately trans disposed relative to C(25) as indicated by the P(1)−Ta(1)−C(25) angle of 160.74(14)°, and so the structure is probably best described as a distorted octahedron rather than a distorted trigonal prism. The Ta−P distance of 2.7713(13) Å in **2** is longer than that observed in the seven-coordinate complex [P_2N_2]$TaMe_3$, where the two Ta−P distances were 2.6180(8) and 2.6088(9) Å.[24] In contrast, both the Ta−N and Ta−Me distances are slightly shorter than those found in [P_2N_2]$TaMe_3$.

The room-temperature ^{1}H NMR spectrum of **2** provides no evidence for the lack of symmetry observed in the solid-state molecular structure, which indicates that there is some fluxional process that occurs in **2**. A single resonance is observed for the three tantalum-bound methyl groups, and there are two silyl methyl environments and two ligand methylene resonances. There is only one set of ortho, meta, and para protons for the nitrogen phenyl groups, and one set of ortho, meta, and para protons for the phosphorus phenyl group. At 185 K, two resonances are observed for the tantalum-bound methyl groups in the ^{1}H NMR spectrum, in a 2:1 ratio, consistent with either an octahedral or trigonal prismatic geometry. Variable-temperature ^{1}H NMR also reveals that the resonances due to the ortho and meta protons of the NPh groups broaden and decoalesce at low temperature, which is indicative of hindered rotation of these phenyl groups. The overlapping nature of these resonances has prevented the accurate determination of kinetic parameters.

Synthesis and Characterization of ([NPN]Ta)$_2$(μ-H)$_4$ (3). The hydrogenation of **2** was performed by adding 4 atm of H_2 gas to a diethyl ether solution of **2**. This reaction is complete within 12 h, which is much faster than the several days required for the complete hydrogenation of [P_2N_2]$TaMe_3$.[25] The solution darkens from pale yellow to dark purple, suggestive of a reduction from Ta(V) to Ta(IV). A single resonance in the room-temperature ^{31}P{^{1}H} NMR spectrum of this species is consistent with a symmetrical structure; this singlet is unchanged even at 180 K. The corresponding ^{1}H NMR spectrum is likewise unchanged by variations in temperature, and the observation of only two silyl methyl resonances is also consistent with a highly symmetrical species. The room-temperature ^{1}H NMR contains the expected ligand resonances, as well as resonance at δ 10.62, which can be assigned to four bridging hydride ligands. This resonance is a broad singlet, with no coupling to ^{31}P resolved. On the basis of these data, a dinuclear structure of the formula ([NPN]Ta)$_2$(μ-H)$_4$ (**3**) is proposed (eq 2).

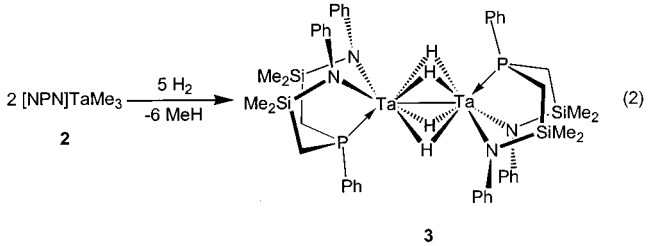

(2)

To date, the solid-state molecular structure of **3** has not been determined by X-ray crystallography. A structure with four bridging hydrides seems probable by comparison to the related species ([P_2N_2]Ta)$_2$(μ-H)$_4$ produced by the hydrogenation of [P_2N_2]$TaMe_3$,[25] as well as from similar structures for other dinuclear Ta(IV) hydrides;[28,29] however, a structure with bridging and terminal hydrides in rapid exchange cannot be entirely

(28) Scioly, A. J.; Luetkens, M. L. J.; Wilson, R. B.; Huffman, J. C.; Sattelberger, A. P. *Polyhedron* **1987**, *6*, 741−757.
(29) Profilet, R. D.; Fanwick, P. E.; Rothwell, I. P. *Polyhedron* **1992**, *11*, 1559−1561.

ruled out from the data obtained from the ^{1}H NMR spectrum. The IR spectra of **3** and the deuterated analogue formed from the reaction of **2** with D_2 (**3**-d_4) contain no absorptions in the region anticipated for a terminal tantalum hydride or tantalum deuteride, respectively.[30] Unfortunately, the region below 1400 cm^{-1}, where bridging hydride or deuteride absorptions would be expected, is obscured by ligand absorptions.

It was possible to provide additional evidence that the structure of **3** contains 4 bridging hydrides by examining the degree of isotopic perturbation of resonance caused by the replacement of hydride ligands with deuteride ligands. The reaction of **2** with a mixture of H_2 and D_2 gas created a series of isotopomers: $([NPN]Ta)_2(\mu\text{-H})_4$, $([NPN]Ta)_2(\mu\text{-H})_3(\mu\text{-D})$, $([NPN]Ta)_2(\mu\text{-H})_2(\mu\text{-D})_2$, $([NPN]Ta)_2(\mu\text{-H})(\mu\text{-D})_3$, and $([NPN]Ta)_2(\mu\text{-D})_4$. This mixture of isotopomers can also be generated by the addition of D_2 gas to **3**. The ^{1}H NMR spectrum of this mixture reveals that the isotopic shifts of the hydride resonances are only very slightly different for each of these isotopomers; the difference in the chemical shift for each is between 0.02 and 0.03 ppm. These data are consistent with the hydrides all occupying bridging positions, rather than there being two different chemical environments for the hydride ligands (bridging and terminal), which should produce a much larger isotopic perturbation of resonance.[31,32]

Synthesis and Characterization of $([NPN]Ta(\mu\text{-H}))_2(\mu\text{-}\eta^1\text{:}\eta^2\text{-}N_2)$ (4). Attempts to crystallize complex **3** under a nitrogen atmosphere resulted in a visible color change. Hydride **3** is dark purple; however, after storage of solutions of **3** under N_2 gas for 1 h at 15 °C, the solution is noticeably lighter colored, and turns brown within 24 h. The brown dinitrogen compound $([NPN]Ta(\mu\text{-H}))_2(\mu\text{-}\eta^1\text{:}\eta^2\text{-}N_2)$ can be isolated in 75% yield from this reaction. The yield can be improved to 90% when this reaction is performed under a 9:1 mixture of N_2 and H_2 gas, as shown in eq 3. The role of H_2 gas in this reaction is under further investigation.

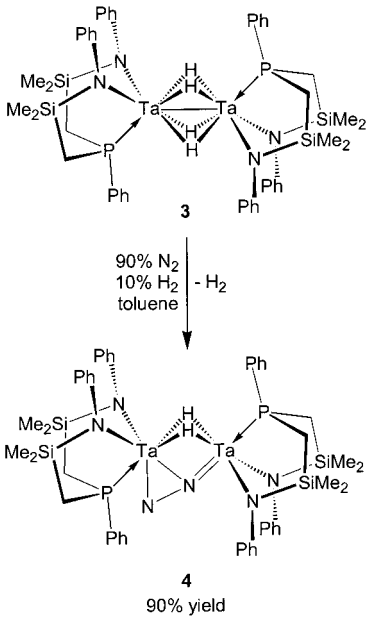

An ORTEP depiction of the solid-state molecular structure of **4** as determined by neutron crystallography is shown in Figure

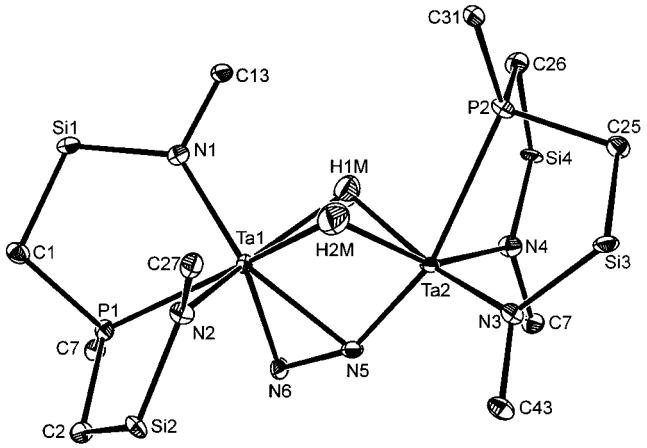

Figure 2. ORTEP depiction of the solid-state molecular structure of $([NPN]Ta(\mu\text{-H}))_2N_2$ (**4**) as determined by neutron crystallography. The silyl methyl groups are omitted for clarity and only the ipso carbons of the PPh and NPh groups and tantalum bound hydrogens are shown. Selected bond lengths (Å), bond angles (deg), and dihedral angles (deg): N(5)−N(6), 1.319(4); Ta(1)−N(5), 2.139(4); Ta(1)−N(6), 1.966(4); Ta(2)−N(5), 1.887(4); Ta(1)···Ta(2), 2.830(4); Ta(1)−P(1), 2.573(5); Ta(2)−P(2), 2.596(5); Ta(1)−N(1), 2.079(4); Ta(1)−N(2), 2.031(4); Ta(2)−N(3), 2.069(4); Ta(2)−N(4), 2.049(4); Ta(1)−HM(1), 2.020(8); Ta(1)−HM(2), 2.016(8); Ta(2)−HM(1), 1.952(7); Ta(2)−HM(2), 1.886(8); Ta(2)−N(5)-N(6), 150.2(2); Ta(1)−N(5)−Ta(2), 89.1(2); Ta(1)−N(6)−N(5), 78.6(2); P(1)−Ta(1)−N(1), 78.8(2); P(1)−Ta(1)−N(2), 77.5(2); P(1)−Ta(1)−N(6), 74.6(2); P(2)−Ta(2)−N(5), 160.3(2); Ta(2)−Ta(1)−P(1), 152.8(2); Ta(2)−Ta(1)−N(1), 122.9(2); Ta(2)−Ta(1)−N(2), 106.9(2); Ta(1)−Ta(2)−P(2), 114.7(2); Ta(1)−Ta(2)−N(3), 128.1(2); Ta(1)−Ta(2)−N(4), 123.4(2); N(1)−Ta(1)−N(2), 108.2(2); N(1)−Ta(1)−N(6), 133.0(2); N(2)−Ta(1)−N(6), P(2)−Ta(2)−N(3), 86.2(2); P(2)−Ta(2)−N(4), 76.3(2); N(3)−Ta(2)−N(4), 107.2(2); N(3)−Ta(2)−N(5), 112.6(2); N(4)−Ta-(2)−N(5), 102.6(2); HM(1)−Ta(1)−HM(2), 60.0(3); HM(1)−Ta(2)−HM(2), 63.4(3); Ta(1)−HM(1)−Ta(2), 90.9(3); Ta(1)−HM(2)−Ta(2), 92.9(2); HM(1)−Ta(1)−Ta(2), 43.6(2); HM(2)−Ta(1)−Ta(2), 41.7(2); HM(1)−Ta(2)−Ta(1), 45.5(2); HM(2)−Ta(2)−Ta(1), 45.3(2); N(1)−Ta(1)−HM(1), 81.4(2); N(1)−Ta(1)−HM(2), 104.7(2); P(1)−Ta(1)−HM(1), 142.4(3); P(1)−Ta(1)−HM(2), 156.7(3); N(2)−Ta(1)−HM(1), 139.5(3); N(2)−Ta(1)−HM(2), 79.6(2); N(3)−Ta(2)−HM(1), 156.8(3); N(3)−Ta(2)−HM(2), 96.5(3); P(2)−Ta(2)−HM(1), 80.2(2); P(2)−Ta(2)−HM(2), 83.2(3); N(4)−Ta(2)−HM(1), 87.8(2); N(4)−Ta(2)−HM(2), 147.3(3); Ta(1)−Ta(2)−N(5)−N(6), 25.8(4); P(1)−Ta(1)−Ta(2)−P(2), −162.6(3).

2 and crystal data are given in Table 2. The corresponding X-ray diffraction data are presented in Table 1. The most intriguing aspect of this structure is the bonding mode of the dinitrogen moiety; it is end-on bound to one tantalum and side-on bound to the other tantalum. In contrast, the majority of dinuclear dinitrogen complexes bind dinitrogen in the end-on mode, particularly derivatives of the group 5 metals.[33−44] This $\mu\text{-}\eta^1\text{:}\eta^2$ bonding mode appears unprecedented in bimetallic

(30) Hlatky, G. G.; Crabtree, R. H. *Coord. Chem. Rev.* **1985**, *65*, 1−48.
(31) Saunders: M.; Telkowski, L.; Kates, M. R. *J. Am. Chem. Soc.* **1977**, *99*, 8070−8071.
(32) Gutiérrez-Puebla, E.; Monge, A.; Paneque, M.; Poveda, M. L.; Taboada, S.; Trujillo, M.; Carmona, E. *J. Am. Chem. Soc.* **1999**, *121*, 346−354.
(33) Fryzuk, M. D.; Haddad, T. S.; Mylvaganam, M.; McConville, D. H.; Rettig, S. J. *J. Am. Chem. Soc.* **1993**, *115*, 2782.
(34) Turner, H. W.; Fellmann, J. D.; Rocklage, S. M.; Schrock, R. R.; Churchill, M. R.; Wasserman, H. J. *J. Am. Chem. Soc.* **1980**, *102*, 7811−7812.
(35) Churchill, M. R.; Wasserman, H. J. *Inorg. Chem.* **1981**, *20*, 2899−2904.
(36) Churchill, M. R.; Wasserman, H. J. *Inorg. Chem.* **1982**, *21*, 218.
(37) Rocklage, S. M.; Turner, H. W.; Fellmann, J. D.; Schrock, R. R. *Organometallics* **1982**, *1*, 703−707.
(38) Rocklage, S. M.; Schrock, R. R. *J. Am. Chem. Soc.* **1982**, *104*, 3077.
(39) Schrock, R. R.; Wesolek, M.; Liu, A. H.; Wallace, K. C.; Dewan, J. C. *Inorg. Chem.* **1988**, *27*, 2050.
(40) Dilworth, J. R.; Henderson, R. A.; Hills, A.; Hughes, D. L.; Macdonald, C.; Stephens, A. N.; Walton, D. R. M. *J. Chem. Soc., Dalton* **1990**, 1077.

Table 2. Crystallographic and Experimental Data for the Neutron Diffraction Study of ([NPN]Ta(μ-H))$_2$(μ-η^1:η^2-N_2) (**4**)

compound	**4**
formula	$C_{48}H_{64}N_6P_2Si_4Ta_2$
fw	1266.00
crystal size, mm	1.8 × 1.2 × 0.9
crystal system	monoclinic
space group	$P2_1/n$
data colln, T (K)	20(2)
a, Å	13.0847(3)
b, Å	19.2086(5)
c, Å	21.1087(5)
β, deg	94.853(2)
V, Å^3	5286.4(2)
Z	4
ρ_{calc}, g cm^{-3}	1.591
wavelength λ, Å	1.5334 (1) (Cu(200) monochromated)
absorption coeff. μ, cm^{-1}	2.469
$2\theta_{max}$, deg	109.9
no. of reflcs (n_o)	10427
no. of indep. reflcns	5918
no. of obsd reflcns [$I > 2.0\ \sigma(I)$]	5194
no. of parameters refined (n_v)	1135
max $\Delta p/\sigma$(p)	<0.1
R_{av}	0.053
R(obs)	0.059
R_{w2}(obs)	0.070
GOF	1.104

[a] $R_{av} = \sum|F_o^2 - F_{o,av}^2|/\sum_i|F_o^2|$. $R = \sum(|F_o - (1/k)F_c|)/\sum|F_o|$. $R_{w2} = [\sum w(F_o^2 - (1/k)F_c^2)^2/\sum w|F_o^2|^2]$, where $w = [\sigma^2(F_o^2) + (0.0394P)^2 + 113.2818P]^{-1}$ and $P = \{[F_o^2 + 2.0(F_c^2)]/3.0\}$GOF $= [\sum_w(F_o^2 - (1/k)F_c^2)^2/(n_o - n_v)]^{1/2}$.

dinitrogen complexes, although similar bonding modes have been observed for the isoelectronic CO and NO^+ and CN^- ligands.[45−48] Related but distinctly different binding modes for N_2 have been found in heterobimetallic complexes of Ni with Li,[49] and Co with K,[50] as well as an unusual titanocene derivative.[51]

The N(5)−N(6) distance of 1.319(4) Å is consistent with a formal assignment of the bridging dinitrogen moiety as (N_2).[4−14,34,37,38,52] The Ta(1)−Ta(2) distance of 2.830(4) Å is short enough for a metal−metal bonding interaction; however, because the two Ta centers are Ta(V) in this formalism, no electrons are available for a metal−metal bonding interaction. The shortest of the tantalum−dinitrogen interactions is the "end-on" Ta(2)−N(5) bond, at 1.887(4) Å. This distance is consistent with the Ta(2)−N(5) bond having considerable double-bond character. The side-on bonding interactions are both longer: the Ta(1)−N(6) bond length is 1.966(4) Å and the Ta(1)−N(5) bond is longer yet at 2.139(4) Å. To compare, the average of the Ta(1)−N(1), Ta(1)−N(2), Ta(2)−N(3), and Ta(2)−N(4) distances is 2.057 Å.

The bridging hydride ligands are unsymmetrically bound to the two tantalum centers, with the Ta(1)−HM(1) and Ta(1)−HM(2) bond distances of 2.020(8) and 2.016(8) Å only slightly longer than the Ta(2)−HM(1) and Ta(2)−HM(2) distances of 1.952(7) and 1.886(8) Å. The Ta(1)−HM(1)−Ta(2) and Ta(1)−HM(2)−Ta(2) bond angles are 90.9(3)° and 92.9(2)°, respectively.

The room-temperature ^{1}H NMR spectrum of dinitrogen complex **4** is indicative of a species of lower symmetry than hydride **3**; however, more symmetry is observed than in the solid-state molecular structure, which exhibits C_1 symmetry. In the room-temperature ^{1}H NMR spectrum four silyl methyl resonances are observed, consistent with a species of C_s symmetry. A single hydride signal is observed at δ 10.85 that is coupled to two different ^{31}P environments and accounts for two hydrides by integration. The chemical shift of the hydride resonance (similar to that observed in **3**) and the coupling of this hydride resonance to both phosphine donors together provide evidence that the two hydride ligands bridge the metal centers. At 190 K, the ^{1}H NMR spectrum is indicative of a less symmetrical species. There are eight silyl methyl resonances, and two bridging hydride resonances, consistent with a species of C_1 symmetry, as was observed in the solid-state molecular structure. Presumably this fluxional process primarily involves the rocking of the [NPN] ligands about the Ta(1)−Ta(2) axis. This is best illustrated by noting the difference between the N(1)−Ta(1)−Ta(2)−P(2) and N(2)−Ta(1)−Ta(2)−P(2) dihedral angles, which are 23.9(3)° and −101.82(19)°, respectively; the N(1)−Ta(1) bond nearly resides in the plane defined by P(2)−Ta(2)−Ta(1), whereas the N(2)−Ta(2) bond is almost perpendicular to this plane. The fluxional process that results in C_s symmetry in the room-temperature ^{1}H NMR spectrum must interchange these environments.

The ^{31}P{^{1}H} NMR spectrum of **4** shows two chemical environments (δ 7.8 and 11.0) and it is unusual for two reasons. First, the resonances are significantly broader than those in hydride **3**, and this broadness is not affected by temperature. This broadness of these peaks is presumably due to the quadrupolar ^{14}N nuclei of the dinitrogen moiety; quadrupolar nuclei are known to cause rapid nuclear spin relaxation, and therefore line broadening.[53] Most unusual about the ^{31}P{^{1}H} NMR spectrum of this product is that although the peak at δ 11.0 is a doublet due to coupling to the second ^{31}P environment, the other peak is apparently a poorly resolved 1:2:2:1 quartet. The presence of an apparent 1:2:2:1 quartet in the ^{31}P{^{1}H} NMR spectrum is consistent with the coupling of this ^{31}P resonance to a single ^{14}N environment ($I = 1$, 99.6% abundance). The coupling constant is coincidentally nearly identical with the coupling constant between the two phosphorus atoms, and combination of a 1:1:1 triplet from coupling to ^{14}N with a 1:1 doublet due to coupling to ^{31}P results in the unusual appearance of the multiplet. The coupling of ^{14}N to ^{31}P is not commonly observed.[54]

Although ^{15}N NMR spectroscopy has been applied to only a minority of dinitrogen complexes,[33,54,55] it should provide a means of identifying the binding mode of dinitrogen in the solution structure of **4**. The ^{15}N NMR spectrum of the isotopically enriched complex ([NPN]TaH)$_2$(μ-η^1:η^2-$^{15}N_2$) (**4**-$^{15}N_2$),

(41) Edema, J. J. H.; Meetsma, A.; Gambarotta, S. *J. Am. Chem. Soc.* **1989**, *111*, 6878−80.
(42) Buijink, J.-K. F.; Meetsma, A.; Teuben, J. H. *Organometallics* **1993**, *12*, 2004.
(43) Berno, P.; Gambarotta, S. *Organometallics* **1995**, *14*, 2159.
(44) Ferguson, R.; Solari, E.; Floriani, C.; Osella, D.; Ravera, M.; Re, N.; Chiesi-Villa, A.; Rizzoli, C. *J. Am. Chem. Soc.* **1997**, *119*, 10104.
(45) Marsella, J. A.; Huffman, J. C.; Caulton, K. G.; Longato, B.; Norton, J. R. *J. Am. Chem. Soc.* **1982**, *104*, 6360.
(46) Aspinall, H. C.; Deeming, A. J.; Donovan-Mtunzi, S. *J. Chem. Soc., Dalton Trans.* **1983**, 2669.
(47) Deeming, A. J.; Donovan-Mtunzi, S. *Organometallics* **1985**, *4*, 693.
(48) Legzdins, P.; Rettig, S. J.; Veltheer, J. E.; Batchelor, J. J.; Einstein, F. W. B. *Organometallics* **1993**, *12*, 3575.
(49) Jonas, K. *Angew. Chem., Int. Ed. Engl.* **1973**, *12*, 997.
(50) Klein, H. F.; Hammer, R.; Weiniger, J.; Friedrich, P.; Huttner, G. *Z. Naturforsch.* **1978**, *33b*, 1267.
(51) Pez, G. P.; Apgar, P.; Crissey, R. K. *J. Am. Chem. Soc.* **1982**, *104*, 482.
(52) Turner, H. W.; Fellmann, J. D.; Rocklage, S. M.; Schrock, R. R.; Churchill, M. R.; Wasserman, H. J. *J. Am. Chem. Soc.* **1980**, *102*, 7809.
(53) Ebsworth, E. A. V.; Rankin, D. W. H.; Cradock, S. *Structural Methods in Inorganic Chemistry*; CRC press: Boston, 1991.
(54) Mason, J. *Chem. Rev.* **1981**, *81*, 205−227.
(55) von Philipsborn, W.; Müller, R. *Angew. Chem., Int. Ed. Engl.* **1986**, *25*, 383−486.

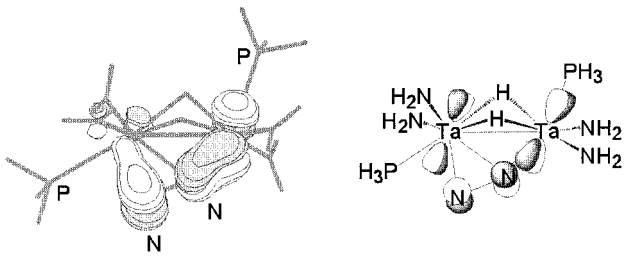

Figure 3. Depiction of an isosurface of the HOMO for model complex **4A** (left) and an illustration clarifying the metal−dinitrogen overlaps in the HOMO (right).

prepared by the addition of $^{15}N_2$ to hydride **3**, contains two chemical shifts for the dinitrogen moiety, separated by 184 ppm. The terminal nitrogen resonance (where terminal refers to N(6) in Figure 3) is a multiplet at δ 163.6 (relative to nitromethane at 0 ppm) with a one-bond coupling to the adjacent ^{15}N of the dinitrogen moiety of 21.5 Hz, a strong coupling to one ligand ^{31}P nucleus (J_{NP} = 21.2 Hz), and a weak coupling to the other ligand ^{31}P nucleus (J_{NP} = 3.5 Hz). The differences in the magnitudes of the couplings to ^{31}P are presumably the result of the former being a two-bond coupling while the latter coupling is through three bonds. The end-on nitrogen resonance (where end-on refers to N(5) in Figure 3) occurs at δ −20.4 and is a multiplet, with the previously mentioned coupling to the adjacent ^{15}N of 21.5 Hz, a strong coupling to one ligand ^{31}P nucleus (J_{NP} = 24.6 Hz), and a weak coupling to the other ligand ^{31}P nucleus (J_{NP} = 6.6 Hz). The difference in magnitude of $^{15}N-^{31}P$ couplings in this case cannot be ascribed to the distance between the nuclei, as these are both two-bond couplings. The larger coupling is due to the ^{31}P nucleus that is trans disposed to the ^{15}N nucleus (P(2) in Figure 2). This $^{15}N-^{31}P$ coupling constant of 24.6 Hz corresponds to a $^{14}N-^{31}P$ coupling constant of 17.5 Hz, due the difference in magnetogyric ratio between these two nuclei, and is consistent with the overlapping multiplet observed in the $^{31}P\{^1H\}$ NMR spectrum of unlabeled **4**.

The loss of H_2 upon binding of dinitrogen is common for the late transition metals;[11,14] however, these reactions do not result in the N_2 moiety being strongly activated. With the early transition metals H_2 loss to generate a dinitrogen complex has been observed with a titanium complex and more recently with a zirconium derivative; however, in both of these examples the N_2 moiety is only weakly bound, and not amenable to further reactivity.[20] No example of H_2 loss to give such a highly activated dinitrogen species has been reported. Typical procedures for the generation of highly activated dinitrogen complexes of the early transition metals involve the use of harsh alkali metal reducing agents, or utilizing transition metal precursors in low oxidation states.[11,12,14] The reaction of **3** with N_2 to produce **4** generates a strongly activated dinitrogen complex without the requirement of strong reducing agents. Of the four electrons involved in the reduction of dinitrogen to form **4**, two are obtained from the elimination of H_2 from **3**, and two are stored in the tantalum−tantalum bond in **3**, which resulted from the reduction of the Ta(V) precursor [NPN]$TaMe_3$ upon hydrogenation. The reduction potentials of the electrons in the tantalum−tantalum bond of the closely related dinuclear tetrahydride $([P_2N_2]Ta)_2(\mu\text{-H})_4$ are known, and are only mildly reducing (−1.18 and −0.33 V relative to the SCE).[25]

Density Functional Theory Analysis of the Bonding in the Side-On End-On Mode. The bonding of dinitrogen in the side-on dinuclear mode and end-on dinuclear mode has been described in detail in the literature.[33,56−58] A density functional theory (DFT) calculation was performed to gain similar insight into the bonding of the N_2 moiety in the new side-on end-on mode. To simplify the calculations the model complex $[(H_3P)(H_2N)_2Ta(\mu\text{-H})]_2(\mu\text{-}\eta^1\text{:}\eta^2\text{-}N_2)$ (**4A**) was studied with restrictions placed on the Ta−Ta−N−H dihedral angles. These restrictions were intended to mimic the rigid geometry imposed by the [NPN] ligand, which prevents the amido donors from freely rotating.

Table 3. Selected Bond Lengths, Bond Angles, and Dihedral Angles for the ab Initio DFT Geometry Optimization of the Model Complex $[(H_3P)(H_2N)_2Ta(\mu\text{-H})]_2(\mu\text{-}\eta^1\text{:}\eta^2\text{-}N_2)$ (**4A**)

atom	atom	distance (Å)	atom	atom	distance (Å)
N(5)	N(6)	1.371	Ta(1)	P(1)	2.820
Ta(1)	N(5)	2.193	Ta(2)	P(2)	2.748
Ta(1)	N(6)	1.988	Ta(1)	N(1)	2.020
Ta(2)	N(5)	1.873	Ta(1)	N(2)	2.005
Ta(1)	Ta(2)	2.891	Ta(2)	N(3)	2.008
			Ta(2)	N(4)	2.023

atom	atom	atom	angle (deg)	atom	atom	atom	angle (deg)
Ta(2)	N(5)	N(6)	152.91	Ta(1)	Ta(2)	P(2)	106.91
Ta(1)	N(5)	Ta(2)	90.29	Ta(1)	Ta(2)	N(3)	126.58
Ta(1)	N(6)	N(5)	79.19	Ta(1)	Ta(2)	N(4)	123.31
P(1)	Ta(1)	N(1)	78.78	N(1)	Ta(1)	N(2)	109.31
P(1)	Ta(1)	N(2)	79.00	N(1)	Ta(1)	N(6)	123.18
P(1)	Ta(1)	N(6)	70.65	N(2)	Ta(1)	N(6)	110.20
P(2)	Ta(2)	N(5)	156.23	P(2)	Ta(2)	N(3)	92.14
Ta(2)	Ta(1)	P(1)	148.84	P(2)	Ta(2)	N(4)	82.61
Ta(2)	Ta(1)	N(1)	120.14	N(3)	Ta(2)	N(4)	108.08
Ta(2)	Ta(1)	N(2)	112.77	N(3)	Ta(2)	N(5)	103.50
				N(4)	Ta(2)	N(5)	108.66

atom	atom	atom	atom	dihedral angle (deg)
Ta(1)	Ta(2)	N(5)	N(6)	8.29
P(1)	Ta(1)	Ta(2)	P(2)	176.18

The geometry of model complex **4A** was optimized (with the exception of the previously stated constraints) with C_1 symmetry by using the Gaussian 98 program[59] and the hybrid functional B3LYP method.[60] The basis functions and effective core potentials (ECP) used were those in the LANL2DZ basis set[61] but with additional d-polarization functions added to P atoms with the exponent of the d-functions set at 0.37. This level of theory has been used previously in the study of metal−metal bonded species and dinuclear tantalum hydride complexes.[25,62]

Selected optimized bond lengths, bond angles, and dihedral angles for the model complex **4A** are shown in Table 3. The numbering scheme used is the same as that for the structure of complex **4** shown in Figure 3. The general features of the optimized geometry of this model complex are in good agreement with the structure of complex **4**, with the exception

(56) Yamabe, T.; Hori, K.; Minato, T.; Fukui, K. *Inorg. Chem.* **1980**, *19*, 2154−2159.
(57) Goldberg, K. I.; Hoffman, D. M.; Hoffmann, R. *Inorg. Chem.* **1982**, *21*, 3863.
(58) Pelikán, P.; Boca, R. *Coord. Chem. Rev.* **1984**, *55*, 55.
(59) Frisch, M. J.; Trucks, G. W.; Schlegel, H. B.; Scuseria, G. E.; Robb, M. A.; Cheeseman, J. R.; Zakrzewski, V. G.; Montgomery, J. A.; Stratmann, R. E.; Burant, J. C.; Dapprich, S.; Millam, J. M.; Daniels, A. D.; Kudin, K. N.; Strain, M. C.; Farkas, O.; Tomasi, J.; Petersson, V. A.; Ayala, P. Y.; Cui, Q.; Morokuma, K.; Malick, D. K.; Rabuck, A. D.; Raghavachari, K.; Foresman, J. B.; Cioslowski, J.; Ortiz, J. V.; Stefanov, B. B.; Liu, G.; Liashenko, A.; Piskorz, P.; Komaromi, I.; Gomperts, R.; Martin, R. L.; Fox, D. J.; Keith, T.; Al-Laham, M. A.; Peng, C. Y.; Nanayakkara, A.; Gonzalez, C.; Challacombe, M.; Gill, P. M. W.; Johnson, B. G.; Chen, W.; Wong, M. W.; Andres, J. L.; Head-Gordon, M.; Repogle, E. S.; Pople, J. A. *Gaussian 98*, Revision A.7; Gaussian, Inc.: Pittsburgh, PA, 1998.
(60) Becke, A. D. *J. Chem. Phys.* **1993**, *98*, 5648.
(61) Hay, P. J.; Wadt, W. R. *J. Chem. Phys.* **1985**, *82*, 270.
(62) Cotton, F. A.; Feng, X. *J. Am. Chem. Soc.* **1997**, *119*, 7514−7520.

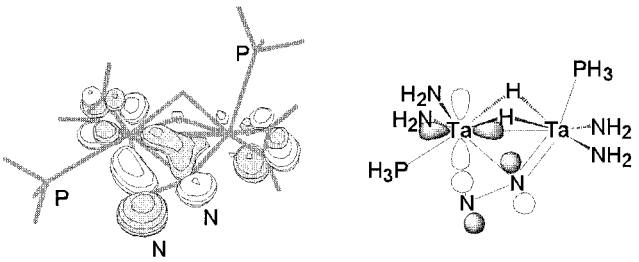

Figure 4. Depiction of an isosurface of the HOMO-1 for model complex **4A** (left) and an illustration clarifying the metal−dinitrogen overlaps in the HOMO-1 (right).

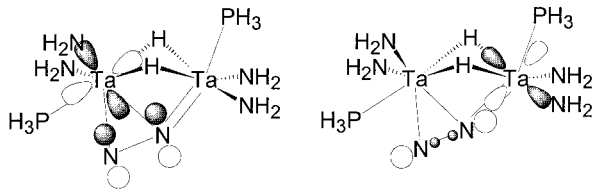

Figure 5. Simplified depictions of the orbital overlaps in the two σ-bonding interactions between the dinitrogen moiety and the tantalum centers in **4A**.

of the longer Ta−P bonds in model **4A**, and a slightly larger Ta(1)−Ta(2) distance. The bond lengths and angles of the dinitrogen moiety are well reproduced, although Ta(1), Ta(2), N(5), N(6), P(1), and P(2) are closer to occupying the same plane in the model complex, which almost gives this model complex a mirror plane of symmetry.

The HOMO of model complex **4A** is shown in Figure 4, and can be described as the π-overlap between two metal-based d-orbitals and a π-antibonding orbital of the dinitrogen moiety. The π-overlap of the rightmost tantalum with the end-on nitrogen (corresponding to Ta(2)−N(5) in Figure 2) is visibly larger than the π-overlap of the leftmost tantalum center with the terminal nitrogen (corresponding to Ta(1)−N(6) in Figure 2). Both the larger contribution of the d-orbital on the rightmost tantalum as well as its orientation relative to the dinitrogen moiety contribute to the greater interaction of this tantalum center with this dinitrogen π-antibonding orbital compared to the leftmost tantalum center.

The HOMO-1 is shown in Figure 4. Similar to the HOMO, the orbital contribution from the dinitrogen moiety is π-antibonding with respect to the N−N bond; however, this π-antibonding contribution is perpendicular to the one present in the HOMO. The dinitrogen-based π-antibonding orbital interacts with a metal-based d-orbital on the leftmost tantalum. Although the rightmost metal center makes the largest π-bonding contribution to the dinitrogen moiety in the HOMO, in the HOMO-1 there is comparatively little contribution from the rightmost metal center; this orbital also contains small contributions from the amido-donor lone-pairs, which are negligible in the HOMO.

The approximate metal−dinitrogen σ-bonding interactions are depicted in Figure 5. The calculated molecular orbitals of model complex **4A** that contain σ-bonding interactions between the metal center and the dinitrogen moiety are complicated by contributions from other orbitals and are much lower in energy than the HOMO and HOMO-1. A depiction of the metal-based d-orbital and dinitrogen-based orbitals in the side-on σ-bonding interaction is shown on the left side of Figure 5, and involves a contribution from the dinitrogen moiety that is π-bonding in nature. The right side of Figure 5 depicts the end-on σ-bonding interaction, which occurs with the dinitrogen-based molecular orbital that is approximately nonbonding in nature.

Scheme 3

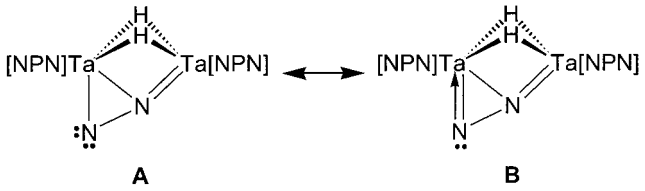

As might be expected, the bonding interactions in the side-on end-on mode contain features of both the side-on and end-on bonding modes of dinitrogen. Unexpectedly absent is a δ-symmetry interaction with the side-on bound dinitrogen moiety, which was anticipated because of the presence of this interaction in side-on bound dinitrogen complexes.[33] Instead, a π-interaction occurs from the terminal nitrogen to the leftmost metal center. These orbital interactions account for the range of Ta−N bond lengths observed for complex **4**. The bonding of the dinitrogen moiety in species **4** can be adequately described by the resonance structures **A** and **B** shown in Scheme 3.

Factors Which Favor the Side-On End-On Bonding Mode for Dinitrogen. The absence of a δ-bonding interaction between the side-on bound dinitrogen and the tantalum center in the calculated molecular orbitals of the model complex **4A** raises the question as to why the side-on end-on bonding mode of dinitrogen is preferred over the end-on dinuclear bonding mode in **4**. One possible explanation is that the bridging hydride ligands force the two tantalum centers so close together that the end-on dinuclear bonding mode becomes impossible. Presumably, the energetic advantage of maintaining bridging hydride ligands outweighs the energy difference between the end-on dinuclear bonding mode and the side-on end-on binding mode. Two complexes are described below that provide evidence that bridging ligands are a requirement for the side-on end-on bonding mode observed in complex **4**.

Reaction of 4 with Propene. The reaction of **4** with propene occurs over a period of two weeks to produce a crystalline red product. A similar reaction with ethylene was observed; however, several unidentified side-products were also generated, and the initial product could not be isolated. The product of the reaction of **4** with propene is $([NPN]Ta(CH_2CH_2CH_3))_2(\mu\text{-}\eta^1\text{:}\eta^1\text{-}N_2)$ (**5**), which results from the insertion of propene into tantalum hydride bonds. This reaction is illustrated in eq 4.

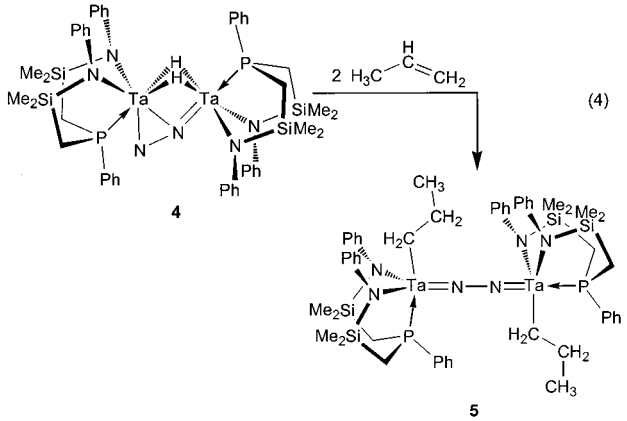

(4)

The solid-state molecular structure of complex **5** as determined by X-ray crystallography is shown in Figure 6, and crystal data are presented in Table 4. As in solution, the solid-state structure of **5** contains two chemically unique tantalum centers, despite the fact that both tantalum centers are coordinated to a

Table 4. X-ray Diffraction Crystal Data and Structure Refinement for ([NPN]Ta($CH_2CH_2CH_3$))$_2$(μ-η^1:η^1-N_2) (**5**), ([NPN]NbCl)$_2$(μ-η^1:η^1-N_2) (**6**), [NPN]Ta(μ-η^1:η^2-N_2CH_2Ph)(μ-H)$_2$TaBr[NPN] (**7**)

compound	**5**[a]	**6**[a]	**7**[a]
formula	$C_{54}H_{76}N_6P_2Si_4Ta_2$	$C_{54}H_{68}Cl_2N_6Nb_2P_2Si_4$	$C_{73}H_{89}N_6P_2BrSi_4Ta_2$
fw	1345.42	1232.18	1666.54
color, habit	red, chip	brown, block	red, prism
cryst size, mm	0.50 × 0.30 × 0.20	0.10 × 0.25 × 0.35	0.60 × 0.40 × 0.20
cryst syst	monoclinic	triclinic	monoclinic
space group	$P2_1/a$ (No. 14)	$P\bar{1}$ (No. 2)	$P2_1/n$ (No. 14)
a, Å	20.2474(6)	11.1226(7)	14.6365(5)
b, Å	12.6106(3)	11.1940(11)	27.3586(7)
c, Å	24.1729(6)	12.6930(14)	18.6731(4)
α, deg		72.592(4)	
β, deg	105.085(2)	81.6611(11)	95.771(2)
γ, deg		81.7194(9)	
V, Å^3	5959.4(3)	1483.5(2)	7439.5(3)
Z	4	1	4
T, °C	−100	−93	−100
ρ_{calc}, g/cm^3	1.50	1.38	1.49
F(000)	2696.00	636.00	3344.00
radiation	Mo	Mo	Mo
μ, cm^{-1}	38.37	6.51	36.25
transmission factors	0.5942−1.0000	0.8455−1.000	0.5919−1.000
$2\theta_{max}$, deg	55.8	61.0	55.8
total no. of reflns	41275	13822	53841
no. of unique reflcns	12334	6821	16114
R_{merge}	0.066	0.041	0.037
no. with $I \geq n\theta(I)$	7481 ($n = 3$)	4483 ($n = 3$)	12522 ($n = 3$)
no. of variables	613	316	801
R	0.060[a]	0.062[a]	0.044[a]
R_w	0.072[a]	0.071[a]	0.068[a]
GOF	0.87	1.21	1.11
max Δ/σ	0.00	0.0004	0.05
residual density, e/Å^3	1.83, −1.51	1.01, −1.06	1.85, −0.93

[a] Rigaku/ADSC CCD diffractometer, $R = \sum||F_o^2| - |F_c^2||/\sum|F_o^2|$; $R_w = (\sum w(|F_o^2| - |F_c^2|)^2/\sum w|F_o^2|^2)^{1/2}$.

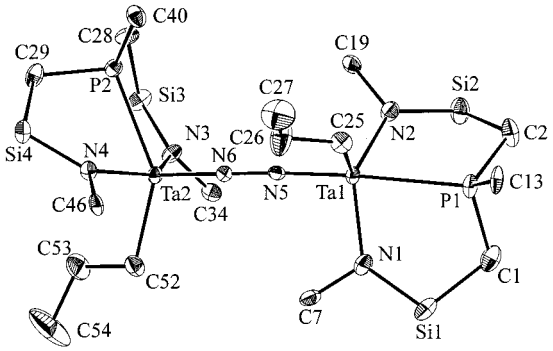

Figure 6. ORTEP depiction of the solid-state molecular structure of ([NPN]Ta($CH_2CH_2CH_3$))$_2$(μ-η^1:η^1-N_2) (**5**) as determined by X-ray crystallography. The silyl methyl groups are omitted for clarity, and only the ipso carbons of the PPh and NPh groups are shown. Selected bond lengths (Å), bond angles (deg), and dihedral angles (deg): N(5)−N(6), 1.289(6); Ta(1)−N(5), 1.818(4); Ta(2)−N(6), 1.815(4); Ta(1)−P(1), 2.734(1); Ta(2)−P(2), 2.640(1); Ta(1)−N(1), 2.057(4); Ta(1)−N(2), 2.061(4); Ta(2)−N(3), 2.092(4); Ta(2)−N(4), 2.061(4); Ta(1)−C(25), 2.194(5); Ta(2)−C(52), 2.193(5); Ta(1)−N(5)−N(6), 174.6(3); N(5)−Ta(1)−P(1), 173.5(1); N(5)−Ta(1)−N(1), 98.2(2);); N(5)−Ta(1)−N(2), 101.5(2); N(5)−Ta(1)−C(25), 98.4(2); P(1)−Ta(1)−N(1), 78.2(1); P(1)−Ta(1)−N(2), 77.3(1); P(1)−Ta(1)−C(25), 88.0(1); N(1)−Ta(1)−N(2), 130.9(2); N(1)−Ta(1)−C(25), 111.5(2); N(2)−Ta(1)−C(25), 109.5(2); Ta(1)−C(25)−C(26), 119.8(4); Ta(2)−N(6)−N(5), 171.8(4); N(6)−Ta(2)−P(2), 109.3(1); N(6)−Ta(2)−N(3), 108.3(2); N(6)−Ta(2)−N(4), 107.3(2); N(6)−Ta(2)−C(52), 108.4(2); P(2)−Ta(2)−N(3), 77.4(1); P(2)−Ta(2)−N(4), 74.6(1); P(2)−Ta(2)−C(52), 142.3(1); N(3)−Ta(2)−N(4), 140.2(2); N(3)−Ta(2)−C(52), 91.7(2); N(4)−Ta(2)−C(52), 93.5(2); Ta(2)−C(52)−C(53), 108.4(4); C(52)−Ta(2)−Ta(1)−C(25), −119.5(4).

[NPN] ligand, a propyl ligand, and an end-on bound dinitrogen unit. The stereochemistry at Ta(1) is best described as trigonal bipyramidal, where the P(1) and N(5) atoms occupy the axial positions, and N(2), N(1), and C(25) occupy the equatorial positions. The stereochemistry at Ta(2) is best described as square-based pyramidal, where the square base is defined by P(2), N(3), C(52), and N(4), and is capped by N(6). The N(5)−Ta(1)−P(1) angle is 175.1(3)° and, in contrast, the N(6)−Ta(2)−P(2) angle is 109.3(1) Å. The Ta(1)−P(1) distance of 2.734(1) Å is significantly longer than the Ta(2)−P(2) distance of 2.640(1) Å, probably due to the strong trans influence of the dinitrogen moiety for the former.

Complex **5** provides an opportunity to compare bond distances in the end-on dinuclear bonding mode of dinitrogen with the side-on end-on mode for electronically similar complexes. The N(5)−N(6) bond length of 1.289(6) Å is not significantly shorter than the N−N bond length in **4** of 1.319(6) Å, which indicates the side-on end-on mode activates dinitrogen to nearly the same degree as the end-on dinuclear mode. On the other hand, the Ta(1)−N(5) and Ta(2)−N(6) distances in **5** are 1.818(4) and 1.815(4) Å, respectively, which are significantly shorter than the end-on Ta(2)−N(5) distance of 1.888(5) Å in **4**, and much shorter than the side-on Ta(1)−N(5) and Ta(1)−N(6) interactions of 2.141(4) and 1.975(5) Å, respectively.

The $^{31}P\{^1H\}$ NMR spectrum of **5** contains two resonances, at δ 14.2 and δ 19.7, that, in contrast to complex **4**, are not coupled. To confirm the bonding mode of dinitrogen, the $^{15}N_2$ labeled species ([NPN]Ta($CH_2CH_2CH_3$))$_2$(μ-η^1:η^1-$^{15}N_2$) was prepared from the reaction of ***4-$^{15}N_2$*** with propene. In the $^{31}P\{^1H\}$ NMR spectrum of ***5-$^{15}N_2$***, the resonance at δ 19.7 is a singlet, whereas the resonance at δ 14.2 is coupled to two different $^{15}N_2$ environments, with coupling constants of 30.5 and 6.6 Hz. The ^{15}N NMR spectrum of ***5-$^{15}N_2$*** contains two doublets of doublets at δ 16.2 and 28.0. The resonance at δ 16.2 is coupled to a single ^{31}P environment, with a $^2J_{PN}$ value

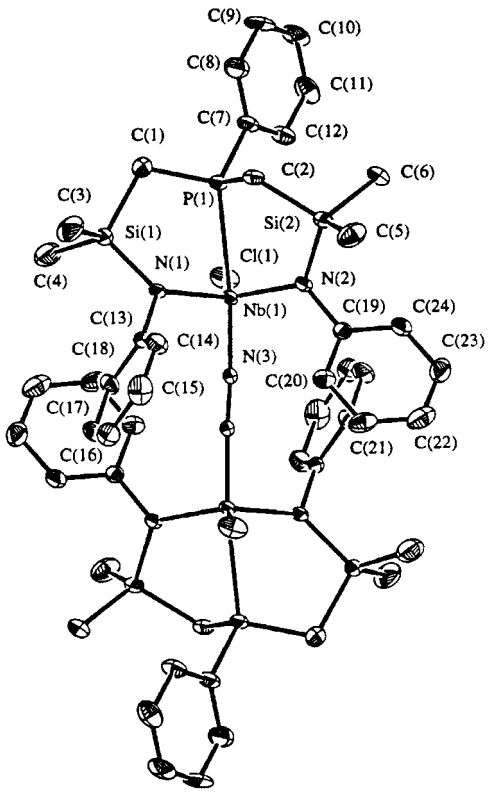

Figure 7. ORTEP depiction of the solid-state molecular structure of ([NPN]NbCl)$_2$(μ-η^1:η^1-N$_2$) (**6**) as determined by X-ray crystallography. Selected bond lengths (Å) and bond angles (deg): N(3)−N(3)*, 1.237(4); N(1)−N(3), 1.843(2); Nb(1)−P(1), 2.7189(8); Nb(1)−N(1), 2.023(2); Nb(1)−N(2), 2.053(2); Nb(1)−Cl(1), 2.3922(9); Nb(1)−N(3)−N(3)*, 176.4(2); P(1)−Nb(1)−N(3), 171.57(8); Cl(1)−Nb(1)−N(3), 99.03(8); N(1)−Nb(1)−N(3), 95.70(9); N(2)−Nb(1)−N(3), 99.44(9); P(1)−Nb(1)−N(1), 76.16(7); P(1)−Nb(1)−N(2) 81.83(7); Cl(1)−Nb(1)−P(1), 87.07(3); Cl(1)−Nb(1)−N(1), 119.31(7); Cl(1)−Nb(1)−N(2) 123.18(7); N(1)−Nb(1)−N(2), 111.59(10).

of 30.5 Hz, as well as to ^{15}N with a $^1J_{NN}$ value 11.3 Hz; the resonance at δ 28.0 also exhibits the identical one-bond coupling to ^{15}N ($^1J_{NN}$ = 11.3 Hz), as well as a two-bond coupling to ^{31}P ($^2J_{PP}$ = 6.6 Hz). The $^1J_{NN}$ value of 11.3 Hz is much smaller than the analogous 21.5 Hz coupling observed for **4**. As noted previously, the N(5)−Ta(1)−P(1) angle is 175.1(3)°, and it is presumably this phosphorus, approximately trans disposed to the dinitrogen moiety, that couples to both the N(5) and N(6) nuclei in the ^{15}N and ^{31}P{^{1}H} spectra of **5**-$^{15}N_2$. The ^{1}H and ^{13}C{^{1}H} NMR spectra are consistent with two ligand and two propyl environments and were assigned with the assistance of a ^{1}H-COSY spectrum and a ^{1}H,^{13}C-HSQC spectrum.

The solution structure of **5** contains only a mirror plane of symmetry, which is consistent with the different geometries observed at the two tantalum centers in the solid-state structure of **5**. This lower symmetry can be explained if the orientation of the [NPN] ligands with respect to the bridging hydrides in **4** is maintained when the propene inserts into the Ta−H bonds to produce **5**. In Figure 6, P(1) is cis disposed to the propyl group, and trans disposed relative to the dinitrogen moiety, so this corresponds to P(2) of complex **4** in Figure 2, which is cis disposed to the bridging hydride ligands and trans disposed to the dinitrogen moiety. Similarly, in Figure 7 P(2) is trans disposed to the propyl group, and cis disposed relative to the dinitrogen moiety, and this corresponds to P(1) in Figure 2. The stereoselectivity of this reaction generates an unsymmetrical dinuclear end-on dinitrogen compound that might not be accessible by other routes; the lack of symmetry in **5** is a direct result of the binding mode of dinitrogen in **4**. More importantly, this compound demonstrates that the bridging hydrides in complex **4** are necessary for maintaining the side-on end-on dinitrogen bonding mode.

Synthesis of ([NPN]NbCl)$_2$(μ-η^1:η^1-N$_2$) (6). In parallel studies, we are examining [NPN] complexes of niobium. The product of the reaction of [NPN]Li$_2$·(THF)$_2$ with NbCl$_3$(DME) is the diamagnetic dinitrogen complex ([NPN]Nb)$_2$(μ-η^1:η^1-N$_2$) (**6**), as shown in eq 5.

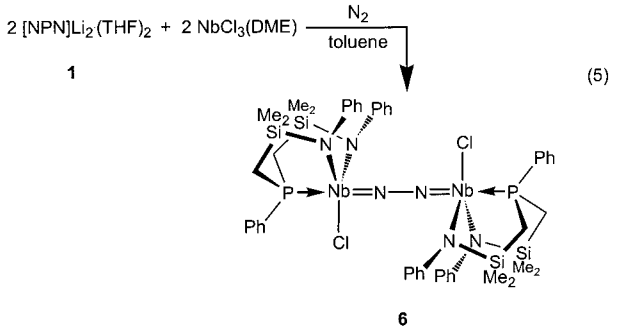

The ^{1}H, ^{13}C{^{1}H}, and ^{31}P{^{1}H} NMR spectra of **6** are consistent with a species of high symmetry. A single resonance is observed in the ^{31}P{^{1}H}NMR spectrum, and only two ligand silyl methyl environments are observed in the ^{1}H NMR spectrum, which is unlike both species **4** and species **5**. The C, H, and N elemental analyses are consistent with a dinitrogen complex.

An ORTEP depiction of the solid-state molecular structure of **6** as determined by X-ray crystallography is shown in Figure 7, and crystal data are presented in Table 4. In the solid-state structure, the two halves of the molecule are related by an inversion center that lies in the middle of the N−N bond. Unlike complex **5**, which is unsymmetrical, the geometry at both Nb centers in **6** is best described as trigonal bipyramidal, with the P(1) phosphine donor and the N(3) atom of the dinitrogen moiety in axial positions and the N(1), N(2), and Cl(1) atoms in equatorial positions. The N(3)−N(3)* bond distance of 1.237(4) Å is slightly shorter than that observed for the dinitrogen moiety in **5** (1.289(6) Å). Although chloride ligands can behave as bridging ligands, they are terminal in **6**; bridging chlorides would require the bonding mode of dinitrogen to change in **6**. The difference in dinitrogen bonding mode between **4** and **6** indicates that not any ligand capable of bridging the metal centers will favor the side-on end-on mode; the side-on end-on bonding mode is presumably less thermodynamically favorable than the end-on dinuclear bonding mode of dinitrogen. Clearly the possible thermodynamic advantage of bridging versus terminal chloride ligands is not sufficient to overcome the thermodynamic disadvantage of the side-on end-on binding mode versus the end-on dinuclear binding mode of dinitrogen, and therefore the end-on dinuclear mode is observed in complex **6**. This example confirms the necessity of a more thermodynamically favored bridging ligand to induce the side-on end-on mode. The hydride ligands perform this role in complex **4**.

Reaction of 4 with Benzylbromide. Does the side-on end-on bonding mode of dinitrogen in complex **4** open up new possibilities for dinitrogen-based reactivity? A simplified picture of the bonding of dinitrogen in this mode has the terminal nitrogen bearing a nonbonding pair of electrons (resonance structure **B** in Scheme 3) and this nitrogen should be expected to react with electrophiles. The availability of nonbonding electrons on the dinitrogen moiety in the side-on end-on mode is a feature shared with the mononuclear end-on and dinuclear

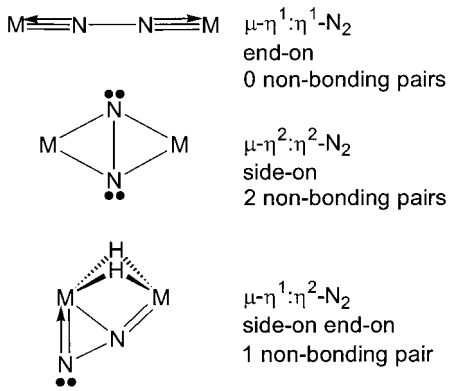

Figure 8. Comparison of the end-on, side-on, and side-on end-on binuclear bonding modes of dinitrogen. Unlike the most prevalent end-on bonding mode, both the side-on and side-on end-on bound dinitrogen moiety bear electron pairs that are nonbonding with respect to the metal centers.

side-on bonding modes of dinitrogen, in contrast to the dinuclear end-on bonding mode. The presence of dinitrogen-based nonbonding electrons should render reactions that form bonds to the dinitrogen moiety more thermodynamically favorable for dinuclear side-on end-on complexes than in dinuclear end-on complexes, where no dinitrogen-based nonbonding electrons are available, and therefore metal−dinitrogen bonding interactions must be broken to form new bonds to the activated dinitrogen moiety. Indeed, many more transformations have been reported for mononuclear end-on bound dinitrogen complexes[11,12,14,63] than dinuclear end-on bound dinitrogen complexes[38] and recent reports confirm the high reactivity of a dinuclear side-on bound N_2 complex.[64] Illustrations of the bonding in the common dinuclear end-on and dinuclear side-on bonding modes are shown in Figure 8, and are compared with the side-on end-on bonding mode with respect to the availability of electron pairs based on the dinitrogen moiety that cannot form bonding interactions to the metal centers.

The reaction of mononuclear dinitrogen compounds with alkylhalides is known, and frequently occurs via a photochemical mechanism.[11,65,66] The benzylation of a dinitrogen complex with benzylbromide appears to be less common; this reaction has only been reported on one occasion,[67] although attempts to perform this reaction with other dinitrogen complexes have been noted.[11,68−70] The reaction of **4** with benzylbromide in toluene occurs over about 8 h at room temperature or within minutes by heating the solution to 70 °C. The extent of the reaction can be monitored visually; initially, the solution is dark brown, which gradually lightens to generate a pale red mixture. The $^{31}P\{^1H\}$ and ^1H NMR spectra are indicative of a single reaction product. The $^{31}P\{^1H\}$ NMR spectrum contains two resonances at δ −0.2 and 12.1 that are coupled (J_{PP} = 22.9 Hz). The ^1H NMR spectrum is indicative of a species with no symmetry, because eight ligand silyl methyl resonances are observed. The two methylene protons of the benzyl fragment appear at δ 5.03 and 5.45 and are coupled to each other with a 13.4 Hz coupling constant. This species can tentatively be assigned as [NPN]Ta(μ-η^1:η^2-N_2CH_2Ph)(μ-H)$_2$TaBr[NPN] (**7**), where a carbon−nitrogen bond has been formed between the terminal nitrogen and the benzyl methylene carbon, and the bromide is transferred to the metal center. This reaction product is shown in eq 6.

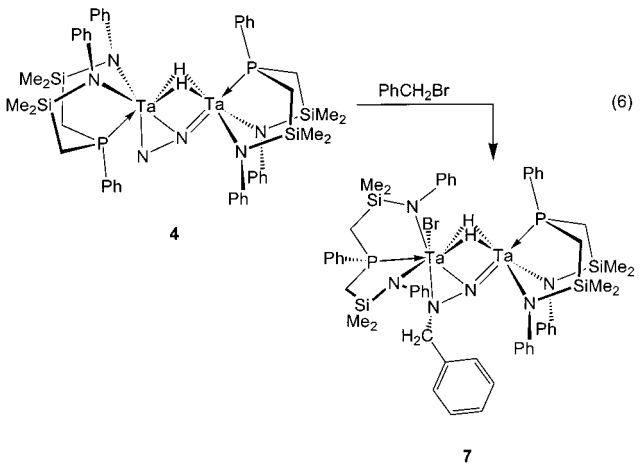

The synthesis of the $^{15}N_2$ labeled species [NPN]Ta(μ-η^1:η^2-$^{15}N_2CH_2Ph$)(μ-H)$_2$TaBr[NPN] (**7-*$^{15}N_2$***) was performed to confirm this assignment. In the ^1H NMR spectrum, one of the two diastereotopic benzyl methylene ^1H resonances is coupled to both ^{15}N nuclei, with coupling constants of 5.0 and 3.2 Hz. The $^{13}C\{^1H\}$ NMR spectrum of **7-*$^{15}N_2$*** provides further evidence that carbon−nitrogen bond formation has occurred. The methylene carbon of the benzyl group appears as a doublet of doublets at δ 69.6, with coupling to both ^{15}N nuclei coincidentally identical at 12 Hz. The $^{31}P\{^1H\}$ spectrum of **7-*$^{15}N_2$*** consists of two coupled resonances at δ −0.2 and 12.1; this latter resonance is also coupled to ^{15}N with a $^2J_{NP}$ value of 27.1 Hz, typical of a ^{31}P nucleus trans disposed to the end-on dinitrogen as in the side-on end-on dinitrogen complexes previously described. The $^{15}N\{^1H\}$ spectrum of **7-*$^{15}N_2$*** contains a resonance for the end-on nitrogen that is a doublet of doublets at δ −45.3, with a 27.1 Hz coupling to the trans disposed ^{31}P nucleus, and a 17.5 Hz coupling to the adjacent ^{15}N nucleus. The second resonance in the $^{15}N\{^1H\}$ NMR spectrum is a doublet at δ −112.4, with a 17.5 Hz coupling to the adjacent ^{15}N nucleus. The J_{NN} coupling constant is much larger for **7-*$^{15}N_2$*** than was observed in **4-*$^{15}N_2$***. The chemical shift of the end-on resonance is very close to that observed in **4-*$^{15}N_2$***; however, the chemical shift of the previously terminal nitrogen is very different than that in **4-*$^{15}N_2$***, and may be characteristic of C−N bond formation.

An ORTEP depiction of the solid-state molecular structure of **7** as determined by X-ray crystallography is shown in Figure 9, and crystal data are presented in Table 4. The X-ray structure of complex **7** demonstrates that the dinitrogen moiety maintains the side-on end-on bonding mode with the two tantalum centers, and also that the terminal nitrogen has formed a bond to carbon. The bromide ligand is attached to the tantalum that is side-on bound to the dinitrogen moiety. The bonding of the dinitrogen moiety to Ta(2) appears largely unchanged relative to the parent complex **4**; the Ta(2)−N(5) bond length of 1.865(3) Å is very similar to that in complex **4** (1.888(5) Å). On the other hand, the Ta(1)−N(5) distance of 2.204(3) Å and the Ta(1)−N(6) distance of 2.102(3) Å are both longer than the analogous

(63) Hidai, M. *Coord. Chem. Rev.* **1999**, *185*−*186*, 99−108.
(64) Fryzuk, M. D.; Love, J. B.; Rettig, S. J.; Young, V. G. *Science* **1997**, *275*, 1445.
(65) Chatt, J.; Diamantis, A. A.; Heath, G. A.; Hooper, N. E.; Leigh, G. J. *J. Chem. Soc., Dalton Trans.* **1977**, 688.
(66) Bossard, G. E.; Busby, D. C.; Chang, M.; George, T. A.; Iske, S. D. A. J. *J. Am. Chem. Soc.* **1980**, *102*, 1001.
(67) Yoshida, T.; Adachi, T.; Ueda, T.; Kaminaka, M.; Sasaki, N.; Higuchi, T.; Aoshima, T.; Mega, I.; Mizobe, Y.; Hidai, M. *Angew. Chem., Int. Ed. Engl.* **1989**, *101*, 1053−5.
(68) Chatt, J.; Dilworth, J. R.; Richards, R. L. *Chem. Rev.* **1978**, *78*, 589.
(69) Chatt, J.; Head, R. A.; Leigh, G. J.; Pickett, C. J. *J. Chem. Soc., Chem. Commun.* **1977**, 299.
(70) The reaction of benzylbromide with Mo and W dinitrogen complexes bearing phosphine ligands results in the formation of bibenzyl, due to the radical pathway by which these complexes react with alkyl halides.

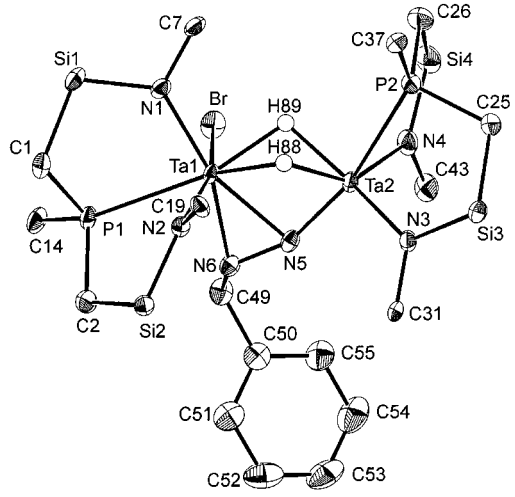

Figure 9. ORTEP depiction of the solid-state molecular structure of [NPN]Ta(μ-η^1:η^2-N_2CH_2Ph)(μ-H)$_2$TaBr[NPN] (**7**) as determined by X-ray crystallography. The silyl methyl groups are omitted for clarity and only the ipso carbons of the PPh and NPh groups are shown. Selected bond lengths (Å), bond angles (deg), and dihedral angles (deg): N(5)−N(6), 1.353(4); Ta(1)−N(5), 2.204(3); Ta(1)−N(6), 2.102(3); Ta(2)−N(5), 1.865(3); Ta(1)−Br, 2.7185(3); N(6)−C(49), 1.466(4); Ta(1)−Ta(2), 2.8449(2); Ta(1)−P(1), 2.6914(8); Ta(1)−P(2), 2.6358(9); Ta(1)−N(1), 2.061(3); Ta(1)−N(2), 2.079(2); Ta(2)−N(3), 2.048(2); Ta(2)−N(4), 2.042(3); Ta(1)−H(88), 1.92(3); Ta(1)−H(89), 1.84(4); Ta(2)−H(88), 1.78(3); Ta(2)−H(89), 1.81(4); Ta(2)−N(5)−N(6), 155.6(2); N(5)−N(6)−C(49), 115.2(3); Ta(1)−N(6)−C(49), 134.3(2); Ta(1)−N(6)−N(5), 75.9(2); P(1)−Ta(1)−N(1), 81.75(8); P(1)−Ta(1)−N(2), 73.02(7); P(1)−Ta(1)−Br, 87.64(2); P(1)−Ta(1)−N(6), 78.44(7); P(1)−Ta(1)−N(5), 114.95(7); N(1)−Ta(1)−N(2), 95.3-(1); N(1)−Ta(1)−Br, 85.56(7); N(1)−Ta(1)−N(5), 161.1(1); N(1)−Ta(1)−N(6), 158.2(1); N(2)−Ta(1)−Br, 160.29(7); P(1)−Ta(1)−H(88), 150.0(9); P(1)−Ta(1)−H(89), 158(1); P(2)−Ta(2)−N(5), 166.80(8); P(2)−Ta(2)−N(3), 84.21(8); P(2)−Ta(2)−N(4), 77.36(9); N(3)−Ta(2)−N(4), 108.8(1); N(3)−Ta(2)−N(5), 104.3(1); N(4)−Ta(2)−N(5), 108.6(1); N(3)−Ta(2)−H(89), 154(1); N(4)−Ta(2)−H(89), 92(1); N(3)−Ta(2)−H(88), 102(1); Ta(2)−N(5)−N(6)−C(49), 142.2(4).

distances in complex **4** (2.141(4) and 1.975(5) Å, respectively). The most dramatic change is the Ta(1)−N(6) distance; this tantalum−nitrogen bond length is consistent with a single bond, compared to the partial double bond character observed in complex **4**. Other features of the solid-state molecular structure of **7** are consistent with the assignment of the Ta(1)−N(6) bond as a single bond. In particular, the bond angles around N(6) are consistent with the presence of a stereochemically active lone pair. The sum of the three bond angles at N(6) is 325.4(7)°, which is much smaller than the 360° anticipated for a planar nitrogen, and quite close to that predicted for tetrahedral bond angles of 109.5°, where the sum of the bond angles would be 328.5°.

The results of this preliminary study indicate that the polarized dinitrogen moiety in complex **4** is susceptible to electrophilic attack at the terminal end of the dinitrogen moiety. Further studies are underway to extend the reactivity of complex **4**.

Conclusions

In this work we document the facile synthesis of a new dinuclear dinitrogen complex with the unprecedented side-on end-on mode of bonding for the N_2 unit. The ditantalum derivative ([NPN]Ta(μ-H))$_2$(μ-η^1:η^2-N_2) results from the direct reaction of N_2 with the dinuclear tetrahydride complex ([NPN]-Ta)$_2$(μ-H)$_4$, which in turn was prepared by the reaction of H_2 with the Ta(V) starting derivative [NPN]TaMe_3. This sequence of reaction is remarkable because it results in the formation of a reactive strongly activated dinitrogen complex of an early transition element without the use of strong reducing agents.[71]

To access the side-on end-on bonding mode requires the availability of donors that can act as efficient bridging ligands; in this system, bridging hydrides are necessary to enforce this unusual ligation. Although chloride ligands are known to bridge, in the closely related niobium system they remain terminal and the ubiquitous end-on bridging N_2 bonding mode is observed in the diniobium derivative ([NPN]NbCl)$_2$(μ-η^1:η^1-N_2). Further substantiation of the crucial role that bridging ligands play in the observation of this side-on end-on mode is the fact that the reaction of ([NPN]Ta(μ-H))$_2$(μ-η^1:η^2-N_2) with propene, which occurs by migratory insertion into the bridging hydride bonds to produce terminal propyl groups, is accompanied by an isomerization to generate the end-on dinitrogen derivative ([NPN]Ta($CH_2CH_2CH_3$))$_2$(μ-η^1:η^1-N_2).

Although reactivity studies of the side-on end-on dinitrogen complex **4** are ongoing, we note that the reaction with benzyl bromide results in the formation of a C−N bond, presumably as a result of the nucleophilic nature of the dinitrogen fragment. The bridging benzylhydrazido fragment remains side-on end-on bound and shows only minor changes in structure from the parent dinitrogen unit. This suggests that the side-on end-on mode of bonding is somewhat robust to those reactions directed at the N_2 moiety, despite precedent for a variety of other binding modes for diazenido ligands (RNN^-) in related dinuclear systems.[72]

Finally, it is useful to speculate on the broader implications of the formation of dinitrogen complex **4**. From the point of view of ultimately generating a catalytic system for the functionalization of dinitrogen, we suggest that this work provides a first step toward this goal because the coordination and activation of the substrate N_2 have been demonstrated to occur in a facile manner. It is also notable that there is a connection to the biological fixation of dinitrogen. It is known that the nitrogenase enzyme produces at least 1 equiv of H_2 gas in the conversion of N_2 to NH_3. Although there is some debate as to whether this arises from a necessary step in this reaction or from a side-reaction of this highly reducing enzyme with H^+,[11,73,74] there is a similarity to the formation of ([NPN]-Ta(μ-H))$_2$(μ-η^1:η^2-N_2) because H_2 is also eliminated for the latter reaction. Does the iron−sulfide−molybdenum core of the nitrogenase enzyme lose H_2 from a hydride intermediate before N_2 binds and is finally reduced? Is so, then our work provides a precedent for this process. Furthermore, it has also been suggested that the electrons that reduce dinitrogen in the iron−sulfide core of nitrogenase are initially stored in metal−metal bonds,[75,76] much like the tantalum−tantalum bonding electrons in hydride **3** that are transferred to dinitrogen to form complex **4**. These ideas must await further details on the biological system.

(71) It should be noted that the precursor $TaMe_3Cl_2$ is prepared from $TaCl_5$ with $ZnMe_2$. This is a metathesis reaction, which results in the formation of $ZnCl_2$. A reducing agent is not necessary to convert Ta(V) to Ta(III) because the 4 electrons required to reduce dinitrogen in complex **4** are obtained by two consecutive *reductive eliminations* of H_2. Reductive elimination reactions allow for metal centers to be reduced in the absence of an added reducing agent.

(72) Schollhammer, P.; Guenin, E.; Petillon, F. Y.; Talarmin, J.; Muir, K. W.; Yufit, D. S. *Organometallics* **1998**, *17*, 1922.

(73) Leigh, G. J. *Sci. Prog. (Oxford)* **1989**.

(74) Sellmann, D.; Fursattel, A. *Angew. Chem., Int. Ed. Engl.* **1999**, *38*, 2023−2026.

(75) Han, J.; Beck, K.; Ockwig, N.; Coucouvanis, D. *J. Am. Chem. Soc.* **1999**, *121*, 10448.

(76) Tyson, M. A.; Coucouvanis, D. *Inorg. Chem.* **1997**, *37*, 33808.

Experimental Section

General Procedures. Unless otherwise stated, all manipulations were performed under an atmosphere of dry oxygen-free dinitrogen by means of standard Schlenk or glovebox techniques (Vacuum Atmospheres HE-553-2 glovebox equipped with a MO-40-2H purification system and a −40 °C freezer). Hexanes were predried by refluxing over CaH_2 and then distilled under argon from sodium benzophenone ketyl with tetraglyme added to solubilize the ketyl. Anhydrous diethyl ether was stored over sieves and distilled from sodium benzophenone ketyl under argon. Toluene was predried by refluxing over CaH_2 and then distilled from sodium under argon. Nitrogen was dried and deoxygenated by passage through a column containing activated molecular sieves and MnO. Deuterated benzene and toluene were dried by refluxing with molten potassium metal and molten sodium metal, respectively, in a sealed vessel under partial pressure, then trap-to-trap distilled and freeze−pump−thaw−degassed three times. Unless otherwise stated, ^1H, ^{31}P, $^1H\{^{31}P\}$, $^{13}C\{^1H\}$, ^{13}C, ^{15}N, $^{15}N\{^1H\}$, and variable-temperature NMR spectra were recorded on a Bruker AMX-500 instrument operating at 500.1 MHz for ^1H spectra. ^1H NMR spectra were referenced to internal C_6D_5H (7.15 ppm) and C_7D_7H (2.09 ppm), $^{31}P\{^1H\}$ NMR spectra to external $P(OMe)_3$ (141.0 ppm with respect to 85% H_3PO_4 at 0.0 ppm), ^{13}C NMR spectra to $^{13}CC_5D_6$ (128.4 ppm), and ^{15}N and $^{15}N\{^1H\}$ spectra to external $^{15}NH_4Cl$ in D_2O (−352.9 ppm with respect to nitromethane at 0.0 ppm). UV−visible spectra were obtained using a Hewlett-Packard 8453 UV−visible spectrophotometer and quartz cuvettes with Teflon valves. Elemental analyses were performed by Mr. P. Borda of this department.

Starting Materials and Reagents. The reagents $PhNH_2$, $ClSiMe_2CH_2Cl$, and $PhCH_2Br$ were purchased from Aldrich and purified by distillation. Solutions of Bu^{n}Li (1.6 M in hexanes) were obtained from Acros Organics and used as received. Hydrogen gas, 10% H_2/N_2 gas mixture, and propene gas were purchased from Praxair. The compounds $TaMe_3Cl_2$,[77] $PhPH_2$,[78] and $NbCl_3(DME)$[79] were prepared by literature methods.

$[NPN]Li_2\cdot(C_4H_8O)_2$ (1). To an ice-cooled stirred solution of aniline (14.9 g, 0.16 mol) in 50 mL of Et_2O and 30 mL of THF was slowly added Bu^{n}Li (100 mL, 1.6 M in hexanes). The resulting colorless solution was stirred for 1 h at room temperature, then cannula transferred dropwise into a stirred solution of $ClSiMe_2CH_2Cl$ in 50 mL of Et_2O at −78 °C. The solution was warmed to room temperature then evaporated to dryness. The residue was dissolved in 100 mL of hexanes and filtered through Celite. The solvent was removed and the remaining oil was distilled under vacuum at 72−74 °C, to afford $PhNHSiMe_2CH_2Cl$ in 90% yield. ^1H NMR (C_6D_6, 20 °C, 200 MHz): δ 0.10 (s, 6H, Si−C*H*$_3$), 2.57 (s, 2H, C*H*$_2$), 3.03 (b, 1H, N*H*), 6.46 (m, 2H, *o-H*), 6.75 (m, 1H, *p-H*), 7.08 (m, 2H, *m-H*).

To an ice-cooled stirred mixture of $PhNHSiMe_2CH_2Cl$ (15.6 g, 0.078 mol) and $PhPH_2$ (4.3 g, 0.5 equiv) in 150 mL of Et_2O was added dropwise 100 mL of Bu^{n}Li (1.6 M in hexanes, 2 equiv). The solution was stirred for 2 h and then thoroughly dried in vacuo. The remaining solids were extracted into 70 mL of toluene and filtered through Celite. The solvent was removed and 20 mL of hexanes was added, to precipitate a white solid from the yellow solution. The addition of an excess of THF (∼4 equiv) initially dissolved the solid, to produce a clear solution. The solution was cooled and over the course of an hour $[NPN]Li_2\cdot(C_4H_8O)_2$ precipitated as a colorless crystalline solid in 85% yield. ^1H NMR (C_6D_6, 25 °C, 500 MHz): δ 0.43 and 0.46 (s, 12H total, Si*CH*$_3$), 1.09 (m, 8H, THF−OCH$_2$C*H*$_2$), 1.24 (m, 4H, PC*H*$_2$Si), 3.31 (m, 8H, THF−OC*H*$_2$CH$_2$), 6.71 (m, 2H, NPh *p-H*), 6.92 (m, 4H, NPh *o-H*), 7.13 (m, 1H, PPh *p-H*), 7.23 (m, 6H, NPh *m-H* and PPh *m-H*), 7.65 (m,2H, PPh *o-H*). $^{31}P\{^1H\}$ NMR (C_6D_6, 25 °C, 500 MHz): δ −37.7 (quartet, $^1J_{PLi}$ = 37.7 Hz). ^7Li NMR (C_6D_6, 25 °C, 500 MHz): δ −1.2 (s, 1Li), −0.9 (d, $^1J_{LiP}$ = 37.7 Hz, 1Li). Anal. Calcd for $C_{32}H_{47}Li_2N_2O_2PSi_2$: C, 64.84; H, 7.99; N, 4.73. Found: C, 65.05; H, 8.02; N, 4.66.

$[NPN]TaMe_3$ (2). A solution of $TaMe_3Cl_2$ (3.51 g, 11.8 mmol) in 50 mL of Et_2O was added dropwise to a −78 °C stirred solution of $[NPN]Li_2\cdot(C_4H_8O)_2$ (7.02 g, 11.8 mmol) dissolved in 800 mL of Et_2O. When the solution was warmed a white precipitate appeared. The solution was evaporated to dryness. The remaining solid was extracted into 80 mL of toluene and filtered through Celite. The solvent was removed and the resulting solid was rinsed with 10 mL of hexanes, which removed a dark brown impurity. The remaining pale yellow solid was dried under vacuum to yield $[NPN]TaMe_3$ (6.33 g, 80%). X-ray quality crystals were obtained by the slow evaporation of a benzene/hexamethyldisiloxane solution and contained 1 equiv of cocrystallized benzene; the crystalline solid rapidly desolvated in the absence of benzene. ^1H NMR (C_6D_6, 30 °C, 500 MHz): δ 0.05, 0.25 (s, 12H total, Si*CH*$_3$), 1.19 (d, $^3J_{PH}$ = 3.4 Hz, 9H, Ta−C*H*$_3$), 1.23, 1.18 (ABX, $^2J_{HH}$ = 14.3 Hz, 4H total, SiC*H*$_2$P), 6.91 (m, 2H, NPh *p-H*), 7.10 (m,4H, NPh *o-H*), 7.12 (m, 5H, PPh *p-H* and NPh *m-H*), 7.18 (m, 2H, PPh *m-H*), 7.58 (m, 2H, PPh *o-H*). $^{31}P\{^1H\}$ NMR (C_6D_6, 30 °C, 500 MHz): δ (ppm) 13.5 (s). $^{13}C\{^1H\}$ NMR (C_6D_6, 30 °C, 500 MHz): δ 1.3 and 3.5 (d, $^3J_{PC}$ = 4.3 and 3.3 Hz, Si(*C*H$_3$)$_2$), 13.9 (d, $^1J_{PC}$ = 6.7 Hz, Si*C*H$_2$P), 69.5 (d, $^2J_{PC}$ = 9.5 Hz, Ta*C*H$_3$), 124.3, 128.3, and 128.9 (s, NPh *o-C*, *m-C*, and *p-C*), 128.8 (d, $^3J_{PC}$ = 8.1 Hz, PPh *m-C*), 130.0 (d, $^4J_{PC}$ = 1.9 Hz, PPh *p-C*), 131.6 (d, $^2J_{PC}$ = 10.5 Hz, PPh *o-C*), 136.6 (d, $^1J_{PC}$ = 17.6 Hz, PPh *i-C*), 149.1 (d, $^4J_{PC}$ = 10.5 Hz, NPh *i-C*). Anal. Calcd for $C_{27}H_{40}N_2PSi_2Ta$: C, 49.08; H, 6.10; N, 4.24. Found: C, 49.26; H, 6.13; N, 4.22

$([NPN]Ta)_2(\mu\text{-}H)_4$ (3). A solution of $[NPN]TaMe_3$ (0.75 g, 1.13 mmol) dissolved in 30 mL of Et_2O was transferred into a 200 mL thick wall glass vessel equipped with a Teflon valve and thoroughly degassed via 3 freeze−pump−thaw cycles. The vessel was cooled in liquid nitrogen and H_2 gas was added. The vessel was then sealed, warmed to room temperature, and stirred for 10 h, over which time the solution turned dark purple. The solvent was removed in vacuo, and the remaining solid dried, to afford $([NPN]_2Ta)_2(\mu\text{-}H)_4$ as a nitrogen-sensitive purple solid in quantitative yield. ^1H NMR (C_6D_6, 30 °C, 500 MHz): δ 0.15, 0.12 (s, 24H total, Si*CH*$_3$), 0.99, 1.05 (ABX, $^2J_{HH}$ = 13.6, 8H, SiC*H*$_2$P), 6.90 (m,4H, NPh *p-H*), 7.21 (m, 6H, PPh *m-H* and *p-H*), 7.26 (m, 8H, NPh *m-H*), 7.33 (m,8H,NPh *o-H*), 7.38 (m, 4H, PPh *o-H*), 10.62 (s, 4H, Ta*H*). $^{31}P\{^1H\}$ NMR (C_6D_6, 20 °C): δ 21.0 (s). Anal. Calcd for $C_{48}H_{66}N_4P_2Si_4Ta_2$: C, 46.67; H, 5.39; N, 4.54. Found: C, 46.23, H, 5.47; N, 4.61.

$([NPN]Ta)_2(\mu\text{-}D)_4$ (3-*d*$_4$). A sample of $([NPN]_2Ta)_2(\mu\text{-}D)_4$ was prepared in a manner identical to that for $([NPN]_2Ta)_2(\mu\text{-}H)_4$ with D_2 gas.

Reaction of $([NPN]Ta)_2(\mu\text{-}H)_4$ with D_2. A NMR tube containing $([NPN]Ta)_2(\mu\text{-}H)_4$ in C_6D_6 was frozen in liquid N_2 and sealed under an atmosphere of D_2 gas. The solvent was thawed and then the sealed NMR tube was transferred into the NMR probe. ^1H NMR, hydride region (C_6D_6, 300 K, 500 MHz): δ 10.61 (s, Ta(μ-D)$_3$(μ-*H*)), 10.59 (s, Ta(μ-D)$_2$(μ-*H*)$_2$), 10.56 (s, Ta(μ-D)$_1$(μ-*H*)$_3$), 10.53 (s, Ta(μ-*H*)$_4$).

$([NPN]Ta(\mu\text{-}H))_2(\mu\text{-}\eta^1\text{:}\eta^2\text{-}N_2)$ (4). A solution of $([NPN]Ta)_2(\mu\text{-}H)_4$ (0.70 g, 0.56 mmol) in 10 mL of Et_2O was exposed to a mixture of 90% N_2 gas with 10% H_2 gas for 24 h, with rapid stirring, resulting in a color change from purple to brown. The solvent was removed and the remaining solid was rinsed with minimal hexanes and dried, to afford $([NPN]_2TaH)_2N_2$ in 90% yield. ^1H NMR (C_6D_6, 30 °C, 500 MHz): δ −0.21, −0.05, 0.02, 0.1 (s, 24H total, Si*CH*$_3$), 0.65 (AMX, $^2J_{HH}$ = 13.5, $^2J_{HP}$ = 10.6, 2H, SiC*H*$_2$P), 1.48 (AMX, $^2J_{HH}$ = 13.5, $^2J_{HP}$ = 12.2, 2H, SiC*H*$_2$P), 1.59, 1.59 (m, 4H total, SiC*H*$_2$P), 6.74 (m, 2H, Ph*H*), 6.83 (b, 2H, PPh *o-H*), 6.89 (m, 2H, Ph*H*), 6.91 (d, 4H, NPh *o-H*), 7.10 to 7.27 (m, 18H, Ph*H*), 8.24 (m, 2H, PPh *o-H*), 10.85 (dd, $^2J_{HP}$ = 20.3, 14.3, 2H, Ta*H*). $^{31}P\{^1H\}$ NMR (C_6D_6, 20 °C): δ 11.0 (d, $^3J_{PP}$ = 21.2 Hz, 1P), 7.8 (m, 1P). Anal. Calcd for $C_{48}H_{64}N_6P_2Si_4Ta_2$: C, 45.71; H, 5.11; N, 6.66. Found: C, 46.05; H, 5.26; N, 6.69.

$([NPN]Ta(\mu\text{-}H))_2{}^{15}N_2$ (4-*^{15}N*$_2$). A solution of $([NPN]Ta)_2(\mu\text{-}H)_4$ (0.30 g, 0.56 mmol) in 5 mL of Et_2O was exposed to $^{15}N_2$ gas, in a manner similar to that used with $([NPN]Ta(\mu\text{-}H))_2N_2$, and afforded $([NPN]TaH)_2{}^{15}N_2$ in 80% yield. No change was observed in the ^1H NMR spectrum. $^{31}P\{^1H\}$ NMR (C_6D_6, 30 °C): δ 11.0 (ABXY, $^3J_{PP}$ = 21.2, J_{PN} = 6.6, J_{PN} = 21.2), 7.8 (ABXY, $^2J_{PP}$ = 21.2, J_{PN} = 3.5, J_{PN} = 24.6). ^{15}N NMR (C_6D_6, 30 °C): δ (ppm) −20.4 (ABXY, J_{NP} = 6.6, J_{NP} = 24.6, J_{NN} = 21.5), 163.6 (ABXY, J_{NP} = 3.5, J_{NP} = 21.2, J_{NN} = 21.5).

$([NPN]Ta(\mu\text{-}D))_2N_2$ (4-*d*$_2$). A sample of $([NPN]Ta(\mu\text{-}D))_2(\mu\text{-}N_2)$ was

(77) Schrock, R. R.; Sharp, P. R. *J. Am. Chem. Soc.* **1978**, *100*, 2389.
(78) Taylor, R. C.; Kolodny, R.; Walters, D. B. *Synth. Inorg. Met.-Org. Chem.* **1973**, *3*, 175−179.
(79) Roskamp, E. J.; Pederson, S. F. *J. Am. Chem. Soc.* **1987**, *109*, 6551.

prepared in a manner identical to that used for ([NPN]Ta(μ-H))$_2$(μ-N_2) with ([NPN]Ta)$_2$(μ-D)$_4$.

([NPN]Ta(CH$_2$CH$_2$CH$_3$))$_2$(μ-η^1:η^1-N_2) (5). A solution of ([NPN]-Ta)$_2$(μ-H)$_2$(μ-η^1:η^2-N_2) (1.10 g, 0.872 mmol) in 50 mL of toluene was added to a glass vessel equipped with a Teflon valve. The vessel was evacuated by 2 freeze−pump−thaw cycles and 1 atm of propene gas was added at room temperature. The vessel was sealed and the solution was stirred. Over the course of two weeks the color changed from dark brown to red. The solvent and excess propene gas were then removed by vacuum and the remaining solid was dissolved in a mixture of hexamethyldisiloxane (4 mL) and benzene (10 mL). Slow evaporation of this solution generated crystalline ([NPN]Ta(CH$_2$CH$_2$CH$_3$))$_2$(μ-η^1:η^1-N_2) (1.04 g, 89%). ^{1}H NMR (C_6D_6, 30 °C, 500 MHz): δ −0.24, 0.04, 0.28, 0.38 (s, 24H total, SiC*H*$_3$), 0.00 (br m, 2H, Ta$_B$C*H*$_2$CH$_2$-CH$_3$), 1.15 and 1.23 (overlapping m, 4H total, SiC*H*$_2$P), 1.16 (overlapping m, 3H, Ta$_B$CH$_2$CH$_2$C*H*$_3$), 1.23 and 1.34 (overlapping m, 4H total, SiC*H*$_2$P), 1.30 (overlapping m, 3H, Ta$_A$CH$_2$CH$_2$C*H*$_3$), 1.78 (overlapping m, 2H, Ta$_B$CH$_2$C*H*$_2$CH$_3$), 1.82 (overlapping m, 2H, Ta$_A$C*H*$_2$CH$_2$CH$_3$), 2.48 (m, 2H, Ta$_A$CH$_2$C*H*$_2$CH$_3$), 6.64 (t, 2H, NPh *p-H*), 6.72 (m, 4H, NPh *m-H*), 6.89 (d, 4H, NPh *o-H*), 6.95 (t, 2H, NPh *p-H*), 7.05 (d, 4H, NPh *o-H*), 7.13 (m, 1H, PPh *p-H*), 7.20 (m, 1H PPh, *p-H*), 7.22 (m, 2H, PPh *m-H*), 7.29 (m, 4H, NPh *m-H*), 7.44 (m, 2H, PPh *m-H*), 7.72 (AMX, 2H, PPh *o-H*), 7.91 (AMX, 2H, PPh *o-H*). ^{31}P{^{1}H} NMR (C_6D_6, 30 °C): δ 14.2 (s, Ta$_A$−*P*), 19.7 (s, Ta$_B$−*P*). ^{13}C{^{1}H} NMR (C_6D_6, 30 °C): δ 0.2, 1.8, and 3.9 (d, Si*C*H$_3$), 5.7 (s, Si*C*H$_3$), 14.7 (d, Si*C*H$_2$P), 17.3 (s, Si*C*H$_2$P), 21.6 (s, Ta$_B$CH$_2$*C*H$_2$-CH$_3$), 22.2 (s, Ta$_B$CH$_2$CH$_2$CH$_3$), 22.7 (s, Ta$_A$CH$_2$CH$_2$*C*H$_3$), 26.0 (s, Ta$_A$-CH$_2$CH$_2$CH$_3$), 59.1 (d, $^2J_{PC}$ = 5.0 Hz, Ta$_A$*C*H$_2$CH$_2$CH$_3$), 76.2 (d, $^2J_{PC}$ = 25.2 Hz, Ta$_B$*C*H$_2$CH$_2$CH$_3$), 121.8 (s, NPh *p-H*), 121.8 (s, NPh *p-H*), 126.2 (s, NPh *o-H*), 127.3 (s, NPh *o-H*), 128.4 (s, NPh *m-H*), 128.5 (s, NPh *m-H*), 129.0 (overlapping d, PPh *m-H*), 129.0 (overlapping d, PPh *m-H*), 130.1 (s, PPh *p-H*), 130.7 (s, PPh *p-H*), 131.7 (d, $^2J_{CP}$ = 12 Hz, PPh *o-H*), 134.1 (d, $^2J_{CP}$ = 15 Hz, PPh *o-H*). HSQC NMR (30 °C,C_6D_6): δ (^{1}H,^{13}C) (−0.24; 0.2), (0.04; 1.8), (0.28; 3.9), (0.38; 5.7), (1.34 and 1.23; 14.7), (1.15 and 1.23; 17.3), (1.78; 21.6), (1.16; 22.2), (1.30; 22.7), (2.48; 26.0), (1.82; 59.1), (0.00; 76.2), (6.64 and 6.95; 121.8), (6.89; 126.2), (7.05; 127.3), (6.72 and 7.29; 128.4 and 128.5), (7.22 and 7.44; 129.0 and 129.0), (7.13; 130.1), (7.20; 130.7), (7.72; 131.7), (7.91; 134.1). COSY NMR (30 °C, C_6D_6): δ (^{1}H;^{1}H) (0.00; 1.78), (1.15; 1.23), (1.16; 1.78), (1.23; 1.34 and 1.15), (1.30; 2.48), (1.34; 1.23), (1.78; 0.00 and 1.16), (1.82; 2.48), (2.48; 1.30 and 1.82), (6.64; 6.72), (6.72; 6.64 and 6.89), (6.89; 6.72), (6.95; 7.29), (7.05; 7.29), (7.13; 7.22), (7.20; 7.44), (7.22; 7.13 and 7.72), (7.29; 6.95 and 7.05), (7.44; 7.20 and 7.91), (7.72; 7.22), (7.91; 7.44). Anal. Calcd for $C_{52}H_{72}N_6P_2Si_4Ta_2$: C, 47.41; H, 5.51; N, 6.38. Found: C, 47.78; H, 5.74; N, 6.41.

([NPN]Ta(CH$_2$CH$_2$CH$_3$))$_2$(μ-η^1:η^1-$^{15}N_2$) (5-$^{15}N_2$). A sample of ([NPN]Ta(CH$_2$CH$_2$CH$_3$))$_2$(μ-η^1:η^1-^{15}N$_2$) (**23-$^{15}N_2$**) was prepared in a manner identical to that for ([NPN]Ta(CH$_2$CH$_2$CH$_3$))$_2$(μ-η^1:η^1-N_2), except with ([NPN]Ta)$_2$(μ-H)$_2$(μ-η^1:η^2-^{15}N$_2$). ^{31}P{^{1}H} NMR (C_6D_6, 30 °C): δ 14.2 (AXY, $^2J_{NP}$ = 30.5 Hz, $^3J_{NP}$ = 6.6 Hz), 19.7 (s). ^{15}N NMR: δ 16.2 (AMX, $^1J_{NN}$ = 11.3 Hz, $^2J_{NP}$ = 30.5 Hz), 28.0 (AMX, $^1J_{NN}$ = 11.3 Hz, $^2J_{NP}$ = 6.6 Hz).

{[NPN]NbCl}$_2$(μ-η^1:η^1-N_2) (6). A room-temperature solution of [NPN]Li$_2$·(C$_4$H$_8$O)$_2$ (2.048 g, 3.455 mmol) in 30 mL of Et$_2$O was added to a slurry of NbCl$_3$(DME) (1.00 g, 3.46 mmol) in 20 mL of Et$_2$O under a N_2 atmosphere. The solution turned brown within a few minutes after being stirred at room temperature. The solution was evaporated to dryness, the remaining solid was extracted into 150 mL of toluene, and the solution was filtered through Celite. The solvent was removed and the remaining material was crystallized from a benzene/hexamethyldisiloxane mixture. The compound {[NPN]NbCl}$_2$(μ-η^1:η^1-N_2)·(C_6H_6) was isolated as a brown crystalline solid (2.98 g, 70%) that is only moderately soluble in aromatic solvents, but has good solubility in THF. The cocrystallized C_6H_6 found present in the crystal structure and identified in the ^{1}H NMR spectrum could not be removed under high vacuum at room temperature. ^{1}H NMR (C_4D_8O, 301.6 K, 500 MHz): δ −0.09, 0.06 (s, 24H total, SiC*H*$_3$), 1.42 (ABX, $^2J_{HH}$ = 13.7 Hz, $^2J_{PH}$ = 8.3 Hz, 4H, SiC*H*$_2$P), 1.59 (ABX, $^2J_{HH}$ = 13.7 Hz, $^2J_{HH}$ = 11.6 Hz, 4H, SiC*H*$_2$P), 6.74 (m, 8H, NPh *o-H*), 6.89 (m,4H, PPh *m-H*), 7.16 (m, 8H, NPh *m-H*), 7.32 (s, 6H, cocrystallized C_6H_6), 7.43 (overlapping m, 6H total, PPh *p-H* and NPh *p-H*), 8.15 (m, 4H, PPh *o-H*). ^{31}P{^{1}H} NMR (C_4D_8O, 301.6 K): δ (ppm) 16.0 (s). ^{13}C{^{1}H} NMR (C_4D_8O, 301.6 K): δ 2.2 (d, Si(*C*H$_3$)$_2$), 2.4 (s, Si(*C*H$_3$)$_2$), 15.0 (m, Si*C*H$_2$P), 122.8, 127.8, 129.1, 129.2, 130.6, and 133.2 (NPh and PPh *o-C*, *m-C*, and *p-C*). Anal. Calcd for $C_{24}H_{31}ClN_3NbPSi_2$·$(C_6H_6)_{0.5}$: C, 52.64; H, 5.56; N, 6.82. Found: C, 52.32; H, 5.64; N, 6.66.

[NPN]Ta(μ-η^1:η^2-N$_2$CH$_2$Ph)(μ-H)$_2$TaBr[NPN] (7). To a dark brown solution of ([NPN]Ta(μ-H))$_2$N$_2$ (1.00 g, 0.793 mmol) in 20 mL of toluene was added a 3-fold excess of benzylbromide. Over the course of 8 h the solution turned dark red. The reaction could also be performed in 5 min by heating the solution to 70 °C. The solvent was removed under vacuum, and the resulting red solid was rinsed with hexanes and cooled to −40 °C. The red solid was collected on a glass filter and dried under high vacuum (1.01 g, 89%) and identified as [NPN]-Ta(μ-η^1:η^2-N$_2$CH$_2$Ph)(μ-H)$_2$TaBr[NPN]. Single crystals suitable for X-ray analysis were obtained by the slow evaporation of a benzene and hexamethyldisiloxane solution. ^{1}H NMR (500 MHz, C_6D_6, 25 °C): δ −0.37, −0.27, −0.05, −0.02, 0.01, 0.14, 0.39, 0.74 (s, 24H total, SiC*H*$_3$), 0.42, 0.81, 1.31, 1.37, 1.40, 1.51, 1.73, 1.90 (ABX, 8H total, SiC*H*$_2$P), 5.03 and 5.45 (AB, $^2J_{HH}$ = 13.4 Hz, 2H total, N$_2$C*H*$_2$-Ph), 5.56 (m, 1H, phenyl proton), 6.48 (m, 1H, phenyl proton), 6.61 (m, 1H, phenyl proton), 6.74 (m, 1H, phenyl proton), 6.79 (d, 2H, phenyl protons), 6.84 (m, 2H, phenyl protons), 6.93 (dd, 2H, PPh o-*H*), 6.97 (d, 2H, phenyl protons), 7.02 (m, 1H, phenyl proton), 7.07−7.2 (overlapping peaks, phenyl protons), 7.25 (m, 1H, phenyl proton), 7.36 (m, 1H, phenyl proton), 7.46 (m, 1H, phenyl proton), 7.59 (m, 1H, phenyl proton), 7.70 (m, 2H, phenyl protons), 8.15 (m, 1H, phenyl proton), 8.46 (dd, 2H, PPh o-*H*), 11.90 (ABXY, $^2J_{HH}$ = 16.3 Hz, $^2J_{HP}$ = 13.0 Hz, $^2J_{HP}$ = 24.9 Hz, 1H, Ta*H*Ta), 13.00 (ABXY, $^2J_{HH}$ = 16.3 Hz, $^2J_{HP}$ = 11.7 Hz, $^2J_{HP}$ = 16.6 Hz, 1H, Ta*H*Ta). ^{31}P{^{1}H} NMR (C_6D_6, 25 °C): δ −0.2 (d, J_{PP} = 23.6 Hz), 12.1 (d, J_{PP} = 23.6 Hz). ^{13}C NMR (C_6D_6, 25 °C): δ 0.5 (d, J_{CP} = 7.1 Hz, Si*C*H$_3$), 1.0 (s, Si*C*H$_3$), 1.1 (d, J_{CP} = 1.1 Hz, Si*C*H$_3$), 1.5 (d, J_{CP} = 1.1 Hz, Si*C*H$_3$), 1.9 (d, J_{CP} = 10.2 Hz, Si*C*H$_3$), 3.0 (d, J_{CP} = 2.7 Hz, Si*C*H$_3$), 4.5 (s, Si*C*H$_3$), 4.8 (d, J_{CP} = 3.3 Hz, Si*C*H$_3$), 14.9, 15.2, 17.3, and 19.4 (s, Si*C*H$_2$P), 69.6 (s, N$_2$-CH$_2$Ph), 122.0 (s, phenyl), 122.3 (s, phenyl), 122.5 (s, phenyl), 124.2 (s, phenyl), 125.6 (s, phenyl), 126.7 (s, phenyl), 127.6 (s, phenyl), 128.3 (s, phenyl), 128.4 (s, phenyl), 128.7 (s, phenyl), 128.8 (s, phenyl), 128.9 (br, phenyl), 129.0 (br, phenyl), 129.3 (br, phenyl), 129.4 (br, phenyl), 129.5 (s, phenyl), 130.1 (d, J_{CP} = 2.2 Hz, phenyl), 130.2 (s, phenyl), 130.5 (d, J_{CP} = 2.2 Hz, phenyl), 133.7 to 133.8 (overlapping peaks, phenyl), 134.6 (d, J_{CP} = 33.2 Hz, PPh), 137.2 (d, J_{CP} = 25.1 Hz, PPh), 144.9 (s, phenyl), 153.2 (d, J_{CP} = 4.9 Hz, phenyl), 154.8 (d, J_{PC} = 4.4 Hz, phenyl), 156.4 (d, J_{PC} = 2.7 Hz, phenyl), 162.3 (d, J_{CP} = 3.8 Hz, phenyl). Anal. Calcd for $C_{55}H_{71}N_6P_2Si_4Ta_2$: C, 46.12; H, 5.00; N, 5.87. Found: C, 46.36; H, 5.24; N, 5.81.

[NPN]Ta(μ-η^1:η^2-^{15}N$_2$CH$_2$Ph)(μ-H)$_2$TaBr[NPN] (7-$^{15}N_2$). The ^{15}N labeled analogue was prepared in a manner identical to that used for the unlabeled material except for using the ^{15}N labeled precursor ([NPN]-TaH)$_2$^{15}N$_2$. ^{1}H{^{31}P} NMR, only peaks affected by coupling to ^{15}N are shown, Lorentz-Gauss enhanced[80] (LB = −5.1, GB = 16.4) (C_6D_6, 25 °C): δ 5.03 (ABXY, $^2J_{HH}$ = 13.4 Hz, J_{HN} = 5.0 Hz, J_{HN} = 3.2 Hz). ^{31}P{^{1}H} NMR (C_6H_6, 25 °C): δ −0.2 (d, $^2J_{PP}$ = 22.9 Hz), 12.1 (dd, $^2J_{PP}$ = 22.9 Hz, $^2J_{PN}$ = 27.1 Hz). ^{15}N{^{1}H} NMR (C_6D_6, 25 °C): δ −35.6 (dd, $^1J_{NN}$ = 18.1 Hz, $^2J_{NP}$ = 27.1 Hz), −112.4 (d, $^1J_{NN}$ = 18.1 Hz). ^{13}C NMR, selected peak only (C_6D_6, 25 °C): δ 69.6 (dd, J_{CN} = 12 Hz, J_{CN} = 12 Hz, N$_2$CH$_2$Ph).

Calculations on [(H$_3$P)(H$_2$N)$_2$Ta(μ-H)]$_2$(μ-η^1:η^2-N$_2$) (4A). The ab initio DFT calculations on the model compound [(H$_3$P)(H$_2$N)$_2$Ta(μ-H)]$_2$(μ-η^1:η^2-N$_2$) were performed with the hybrid functional B3LYP method[60] with use of the Gaussian 98 package.[59] The basis functions and effective core potentials (ECP) used were those in the LANL2DZ basis set developed by Hay and Wadt[61] and provided with the Gaussian 98 program, but with an additional *d* polarization function added to P atoms. The exponent of the *d* function was 0.37. This level of theory has been shown to be adequate for modeling complexes containing metal−metal bonds of various orders.[62] Model complex **4A** was

(80) Braun, S.; Kalinowski, H.-O.; Berger, S. *150 and More Basic NMR Experiments*; Wiley-VCH: Toronto, 1998.

optimized with C_1 symmetry. Orbital depictions were created with use of the MOLDEN program.[81]

X-ray Crystallographic Analyses. Crystallographic data appear in Table 1 for **2** and **4** and in Table 4 for **5**, **6**, and **7**. All measurements were made on a Rigaku/ADSC CCD area detector with graphite monochromated Mo Kα radiation. The final unit-cell parameters were obtained by least-squares methods on the setting angles for 19510 reflections (**2**), 6013 reflections (**4**), 18889 reflections (**5**), 9572 reflections (**6**), and 31949 reflections (**7**). The data were processed[82] and corrected for Lorentz and polarization effects. Structures **4**, **5**, and **7** were solved by direct methods[83] and expanded by using Fourier[84] techniques. Structures **2** and **6** were solved by heavy atom Patterson methods[85] and also expanded by using Fourier[84] techniques. All non-hydrogen atoms were refined with anisotropic thermal parameters. The tantalum bound hydrogen atoms in **4** could not be located and were omitted from the model. The tantalum bound hydrogen atoms in **7** were located in a difference map and refined with isotropic thermal parameters. All remaining hydrogen atoms were fixed in calculated positions with C−H = 0.98 Å. Neutral atom scattering factors and anomalous dispersion corrections were taken from the *International Tables for X-ray Crystallography*.[86,87] Atomic coordinates, anisotropic thermal parameters, complete bond lengths and bond angles, torsion angles, intermolecular contacts, and least-squares planes are included as Supporting Information.

Neutron Diffraction Study of ([NPN]Ta(μ-H))$_2$(μ-η^1:η^2-N$_2$) (4). A dark brown, transparent, platelike crystal of **4**, of volume 1.8 mm^3, obtained by slow evaporation of a toluene solution, was glued (using the two component glue Kwikfill) on a vanadium pin under a nitrogen atmosphere and then sealed in a SiO_2 thin-walled capillary. The sample was transferred to a DISPLEX cryorefrigerator[88] on the thermal-beam instrument D19, at the ILL reactor, equipped with a 4° × 64° position sensitive detector.[89] A Cu(200) monochromator in reflection (nominal takeoff angle 75°) was used to select a neutron beam of wavelength 1.5334(1) Å.

The sample was slowly cooled (∼1 °C/min) to 20 K, while monitoring the strong 2 1 −2 reflection. No change in mosaic or splitting of the peak was observed. The room-temperature space group $P2_1/n$ was confirmed at 20 K.

Reflections were measured (using the ILL programs Hklgen and Mad) to pre-set monitor counts, in equatorial or normal-beam geometry, using ω scans. The time per step in ω increased with the scattering angle to 10 s per step at high scattering angle. Most of the unique reflections up to $2\theta \cong 100°$ were recorded and some further reflections were measured up to $2\theta \cong 110°$. Three standard reflections were monitored regularly, and showed no significant variation.

The unit cell dimension were precisely determined from the centroids in 3D of 3176 strong reflections (in the range $3.1 \leq \theta \leq 54.95°$) by using the program Rafd19, and the collected intensities were integrated in 3D by using the program Retreat developed at ILL.[90] In view of the small size of the crystal and of the small value of the μ coefficient, no absorption correction was necessary. Further crystallographic data and experimental details are summarized in Table ZZ and Table SN1 in the Supporting Information.

The starting structural model for the refinement was based on the atomic coordinates for the heavy atoms taken from the X-ray structural determination. The structure was refined by full matrix least squares, minimizing the function $[\sum w(F_o^2 - (1/k)F_c^2)^2]$ and using all independent data. During the refinement the Fourier difference maps clearly revealed all the H atoms positions of the ligand and showed clearly two negative peaks between the two Ta atoms, corresponding to the bridging hydride ligands. The final structure model included coordinates and anisotropic displacement parameters for all atoms. No extinction correction was deemed necessary. Upon convergence the final Fourier difference map showed no significant features. The coherent scattering amplitudes used were those tabulated by Sears.[91] All calculations were carried out by using the PC version of the SHELX-97 programs.[92]

Acknowledgment. We gratefully acknowledge both the NSERC of Canada and the Petroleum Research Fund, administered by the American Chemical Society, for funding in the form of research grants. Financial support was also provided by the NSERC of Canada in the form of a postgraduate scholarship for S. A. Johnson, as well as the University of British Columbia in the form of a University Graduate Fellowship.

Supporting Information Available: Full experimental details, tables of parameters, fractional coordinates and thermal parameters, bond lengths, bond angles, torsion angles, and ORTEP diagrams for the X-ray structures of **1**, **2**, **4**, **5**, **6**, and **7** as well as for the neutron structure of **4**; density functional theory calculation results for model complex **4A** (PDF). This material is available free of charge via the Internet at http://pubs.acs.org.

JA0041371

(81) Schaftenaar, G. *Molden*, 3.5 ed.; CAOS/CAMM Center, University of Nijmegen, The Netherlands, 1991.

(82) *teXsan: Crystal Structure Analysis Package*; Molecular Structure Corp.: The Woodlands, TX, 1996.

(83) Altomare, A.; Burla, M. C.; Cammali, G.; Cascarano, M.; Giacovazzo, C.; Guagliardi, A.; Moliterni, A. G. G.; Polidori, G.; Spagna, A. *SIR97*, an integrated package of computer programs for the solution and refinement of crystal structures using single-crystal data, 1999.

(84) Beurkens, P. T.; Admiraal, G.; Beurskens, G.; Bosman, W. P.; de Gelder, R.; Israel, R.; Smits, J. M. M. *DIRDIF94*; The DIRDIF-94 program system, Technical Report of the Crystallography Laboratory, University of Nijmegen, The Netherlands, 1994.

(85) Beurskens, P. T.; Admiraal, G.; Beurskens, G.; Bosman, W. P.; Garcia-Granda, S.; Gould, R. O.; Smits, J. M. M.; Smykalla, C. *PATTY*; The DIRDIF program system, Technical Report of the Crystallography Laboratory, University of Nijmegen, The Netherlands, 1992.

(86) *International Tables for X-ray Crystallography*; Kynoch Press: Birmingham, U.K. (present distributor Kluwer Academic: Boston, MA), 1974; Vol. IV.

(87) *International Tables for Crystallography*; Kluwer Academic: Boston, MA, 1992; Vol. C.

(88) Archer, J.; Lehmann, M. S. *J. Appl. Crystallogr.* **1986**, *19*, 456−458.

(89) Thomas, M.; Stansfield, R. F. D.; Berneron, M.; Filhol, A.; Greenwood, G.; Jacobe, J.; Feltin, D.; Mason, S. A. *Position-Sensitive Detection of Thermal Neutrons*; Academic Press: London, 1983.

(90) Wilkinson, C.; Khamis, H. W.; Stansfield, R. F. D.; McIntyre, G. J. *J. Appl. Crystallogr.* **1988**, *21*, 471−478.

(91) Sears, V. F. *Neutron News* **1992**, *3*, 26−27.

(92) Sheldrick, G. M. *SHELX-97*, Structure Solution and Refinement Package; Georg-August Universität Göttingen, 1997.